Technical Report Documentation Page

1. Report No.	2. Government Accession No.	3. Recipient's Catalog No.
CA14-2173		

4. Title and Subtitle	5. Report Date
Influence of the Spacing of Longitudinal Reinforcement on the Performance of Laterally Loaded CIDH Piles – Experimental Investigation	10/20/2014
	6. Performing Organization Code

7. Author(s)	8. Performing Organization Report No.
Vasileios Papadopoulos and P. Benson Shing	UCSD/SSRP-14/08

9. Performing Organization Name and Address	10. Work Unit No. (TRAIS)
Department of Structural Engineering University of California, San Diego 9500 Gilman Drive, Mail Code 0085 La Jolla, California 92093-0085	11. Contract or Grant No. 65A0369

12. Sponsoring Agency Name and Address	13. Type of Report and Period Covered
California Department of Transportation Division of Engineering Services 1801 30th St., MS #9-2/5I Sacramento, California 95816	Technical Report
	14. Sponsoring Agency Code

15. Supplementary Notes

Prepared in cooperation with the State of California Department of Transportation.

16. Abstract

In the presence of ground water, the slurry displacement method is normally used for the placement of concrete during the construction of cast-in-drilled-hole (CIDH) piles to ensure the stability of the drilled hole before concrete placement. When concrete is placed under water without compaction, defects or cavities may occur, affecting the structural integrity of the pile. In this situation, non-destructive testing, such as gamma-gamma testing, is to be conducted to detect potential anomalies in the concrete. These tests require the placement of inspection (PVC) tubes inside the pile. To accommodate the inspection tubes, the center-to-center spacing of the adjacent longitudinal bars in the pile has to be larger than the 8-in. maximum permitted by the Caltrans Bridge Design Specifications and the AASHTO LRFD Bridge Design Specifications. The impact of this increased spacing on the structural performance of the pile was not well understood.

This report presents an experimental study that investigated the effect of the circumferential spacing of longitudinal reinforcement in CIDH piles on their structural performance. In this study, two 28-in.-diameter piles were tested under a constant vertical compressive load with lateral displacement cycles of increasing amplitudes. The two specimens had the same quantity and spacing of transverse reinforcement and similar quantities of longitudinal reinforcement. Specimen #1 had 6 #11 longitudinal bars spaced at 11 in. on center, which exceeded that maximum spacing permitted by the current design specifications. Specimen #2 had 10 #9 bars spaced at 6.75 in. on center. The total cross-sectional area of the longitudinal steel in Specimen #1 was 1.52% of that of the pile, while it was 1.62% in Specimen #2.

The experimental results have shown that the spacing of longitudinal bars in circular RC members can be larger than 8 in. without a detrimental effect on structural performance. This spacing does not affect the effectiveness of the confinement on the concrete core and the ductility of the member. However, the results have shown that the diameter of longitudinal bars can affect the flexural ductility of a member. Flexural ductility in a plastic-hinge zone is often limited by the buckling of the longitudinal bars after the spalling of the concrete cover, which leads to severe bar strains causing the fracture of the bars. Larger-diameter bars have better buckling resistance for the same spacing of the transverse reinforcement, and can therefore result in more ductile flexural behavior. Furthermore, the spacing and the diameter of longitudinal bars have a clear influence on the spacing and the width of flexural cracks. Increasing the diameter and the spacing of longitudinal bars can lead to wider crack spacing and larger crack widths as also shown in other studies.

17. Key Words	18. Distribution Statement
CIDH piles, reinforcement spacing, slurry displacement method, vertical reinforcement, ductility, confinement, crack spacing, crack width, inspection tubes	No restrictions. This document is available to the public through the National Technical Information Service, Springfield, Virginia 22161.

19. Security Classification (of this report)	20. Security Classification (of this page)	21. No. of Pages	22. Price
Unclassified	Unclassified	77	

STRUCTURAL SYSTEMS

RESEARCH PROJECT

Report No.
SSRP-14/08

Influence of the Spacing of Longitudinal Reinforcement on the Performance of Laterally Loaded CIDH Piles – Experimental Investigation

by

Vasileios Papadopoulos
P. Benson Shing

Report Submitted to the California Department of Transportation under Contract No. 65A0369

October 2014

Department of Structural Engineering
University of California, San Diego
La Jolla, California 92093-0085

University of California, San Diego
Department of Structural Engineering
Structural Systems Research Project
Report No. SSRP-14/08

Influence of the Spacing of Longitudinal Reinforcement on the Performance of Laterally Loaded CIDH Piles – Experimental Investigation

by

Vasileios Papadopoulos
Graduate Student Researcher

P. Benson Shing
Professor of Structural Engineering

Final Report Submitted to the California Department of Transportation under Contract No. 65A0369

Department of Structural Engineering
University of California, San Diego
La Jolla, California 92093-0085

October 2014

Disclaimer

This document is disseminated in the interest of information exchange. The contents of this report reflect the views of the authors who are responsible for the facts and accuracy of the data presented herein. The contents do not necessarily reflect the official views or policies of the State of California or the Federal Highway Administration. This publication does not constitute a standard, specification or regulation. This report does not constitute an endorsement by the California Department of Transportation of any product described herein.

For individuals with sensory disabilities, this document is available in Braille, large print, audiocassette, or compact disk. To obtain a copy of this document in one of these alternate formats, please contact: the Division of Research and Innovation, MS-83, California Department of Transportation, P.O. Box 942873, Sacramento, CA 94273-0001.

Acknowledgments

Funding for the investigation presented in this report was provided by the California Department of Transportation (Caltrans) under Contract No. 65A0369. The authors are most grateful to Caltrans engineers for their continuous technical input and advice throughout this study. Dr. Charles Sikorsky of Caltrans was the project manager, who provided unfailing support and guidance to assure the successful completion of this study.

The experiments presented in this report were conducted in the Charles Lee Powell Structural Engineering Laboratories at the University of California at San Diego. The authors would like to express their sincere gratitude to the laboratory staff, especially Dr. Christopher Latham, for their professionalism and high-quality technical work.

Abstract

In the presence of ground water, the slurry displacement method is normally used for the placement of concrete during the construction of cast-in-drilled-hole (CIDH) piles to ensure the stability of the drilled hole before concrete placement. When concrete is placed under water without compaction, defects or cavities may occur, affecting the structural integrity of the pile. In this situation, non-destructive testing, such as gamma-gamma testing, is to be conducted to detect potential anomalies in the concrete. These tests require the placement of inspection (PVC) tubes inside the pile. To accommodate the inspection tubes, the center-to-center spacing of the adjacent longitudinal bars in the pile has to be larger than the 8-in. maximum permitted by the Caltrans Bridge Design Specifications and the AASHTO LRFD Bridge Design Specifications. The impact of this increased spacing on the structural performance of the pile was not well understood.

This report presents an experimental study that investigated the effect of the circumferential spacing of longitudinal reinforcement in CIDH piles on their structural performance. In this study, two 28-in.-diameter piles were tested under a constant vertical compressive load with lateral displacement cycles of increasing amplitudes. The two specimens had the same quantity and spacing of transverse reinforcement and similar quantities of longitudinal reinforcement. Specimen #1 had 6 #11 longitudinal bars spaced at 11 in. on center, which exceeded that maximum spacing permitted by the current design specifications. Specimen #2 had 10 #9 bars spaced at 6.75 in. on center. The total cross-sectional area of the longitudinal steel in Specimen #1 was 1.52% of that of the pile, while it was 1.62% in Specimen #2.

The experimental results have shown that the spacing of longitudinal bars in circular RC members can be larger than 8 in. without a detrimental effect on structural performance. This spacing does not affect the effectiveness of the confinement on the concrete core and the ductility of the member. However, the results have shown that the diameter of longitudinal bars can affect the flexural ductility of a member. Flexural ductility in a plastic-hinge zone is often limited by the buckling of the longitudinal bars after the spalling of the concrete cover, which leads to severe bar strains causing the fracture of the bars. Larger-

diameter bars have better buckling resistance for the same spacing of the transverse reinforcement, and can therefore result in more ductile flexural behavior. Furthermore, the spacing and the diameter of longitudinal bars have a clear influence on the spacing and the width of flexural cracks. Increasing the diameter and the spacing of longitudinal bars can lead to wider crack spacing and larger crack widths as also shown in other studies.

Table of Contents

List of Figures

List of Tables

1 Introduction

1.1 Background

In the presence of ground water, the slurry displacement method is normally used for the placement of concrete during the construction of cast-in-drilled-hole (CIDH) piles to ensure the stability of the drilled hole before concrete placement. When concrete is placed under water without compaction, defects or cavities may occur, affecting the structural integrity of the pile. Hence, the construction of CIDH piles larger than 2 ft. in diameter under wet conditions requires the installation of inspection (PVC) tubes for non-destructive detection of potential anomalies in the concrete using methods such as gamma-gamma testing, as shown in Figure 1.1. Normally, one inspection tube is required per foot of pile diameter. The inspection tubes are placed in contact with the outermost hoops, along the same circumference as that of the longitudinal bars, as shown in the figure. Since the clear spacing between a tube and an adjacent bar needs to be 3 in. to permit a good flow of the concrete paste, the clear spacing between the longitudinal reinforcing bars immediately adjacent to a tube has to be 8.5 in. Hence, the placement of inspection tubes will result in the violation of the maximum allowable center-to-center spacing of 8 in. for longitudinal bars, as specified in the Caltrans Bridge Design Specifications (Caltrans 2003) and the AASHTO LRFD Bridge Design Specifications (AASHTO 2010).

A study was carried out to investigate the effect of the large spacing (greater than 8 in.) of longitudinal reinforcement on the structural performance of a pile. The study consisted of both experimental and analytical investigations. This report focuses on the experimental study and its findings.

1.2 Past Research

The influence of the quantity and spacing of transverse reinforcement on the ductility and structural performance of RC members subjected to axial and flexural loads has been well studied and understood. However, there is only limited information on the influence of the spacing of longitudinal reinforcement

on the structural performance of an RC member. It has been perceived that the spacing of longitudinal bars has a certain influence on the effectiveness of the confinement provided by transverse reinforcement. While this can be understood for members with rectangular sections, in which the spacing of the cross-ties is normally related to the spacing of the longitudinal bars, it is less so for circular members. Pauley and Priestley (1992) have recommended that this spacing be no greater than 8 in. for both rectangular and circular columns. They have stated that this could lead to better confined concrete, but they have also pointed out that there is no compelling justification for this recommendation. Both Caltrans (2003) and AASHTO (2010) have specified the spacing limit of 8 in. for compression members. Nevertheless, from the structural performance standpoint, the spacing limit for the longitudinal bars in a circular member should depend on the diameter of the member, and it is reasonable to expect that a member with a larger diameter can have a larger circumferential spacing of the longitudinal bars without affecting its structural performance. However, before the study reported here, there was no experimental data available to support or discourage the use of longitudinal bar spacing greater than 8 in.

Parameters that may influence the confinement effect in a circular RC member include: (a) the longitudinal steel ratio, ρ_l, (b) the transverse reinforcement ratio, ρ_t, (c) the angular spacing, θ_l, and the circumferential spacing, s_l, of the longitudinal bars, (d) the spacing, s_t, of the transverse steel, (e) the yield strength of the steel, and (f) the compressive strength of the concrete. This report focuses on the impact of the circumferential spacing of the longitudinal bars. The influence of the transverse reinforcement has been well studied and will not be considered here.

The impact of the spacing of longitudinal bars on the seismic performance of a bridge column or pile was not well understood. It has been perceived that larger spacing may negatively affect the efficiency of the confinement on concrete and, thereby, reduce the flexural ductility of the member (Pauley and Priestley 1992). However, limited experimental data obtained by Mander et al. (1988b) has shown that the influence of the spacing of longitudinal bars on the behavior of circular RC columns under compression is almost negligible as shown in Figure 1.2. Neverthless, the maximum center-to-center spacing of longitudinal bars considered in their study was less than 6.5 in. For rectangular columns, a closer spacing

of longitudinal bars has a clear benefit of enhancing the compressive strength and ductility, as shown in Figure 1.3. However, for rectangular columns, a closer spacing of longitudinal bars also means a closer spacing of cross-ties, which results in a better arching action and a more effectively confined concrete as illustrated in Figure 1.4.

1.3 Scope of this Study and Organization of the Report

In this study, two pile specimens were tested in the Powell Structural Engineering Laboratory at the University of California at San Diego to investigate the impact of having the spacing of longitudinal bars greater than 8 in. on the structural performance of piles. One specimen was designed according to the Caltrans Bridge Design Specifications (Caltrans 2003) and the AASHTO LRFD Bridge Design Specifications (AASHTO 2010). The other had the same design except that its longitudinal reinforcement had spacing much greater than 8 in., violating the current design requirements. The experimental program and findings are presented in this report.

Chapter 2 of this report describes the experimental program, including the design of the test specimens, the test setup, the testing procedure, and the instrumentation scheme. Chapter 3 presents the test results and observations. Finally, a summary and the conclusions of this study are provided in Chapter 4.

Figure 1.1 – Typical drilled shaft reinforcing cage with PVC inspection tubes (Alter 2011)

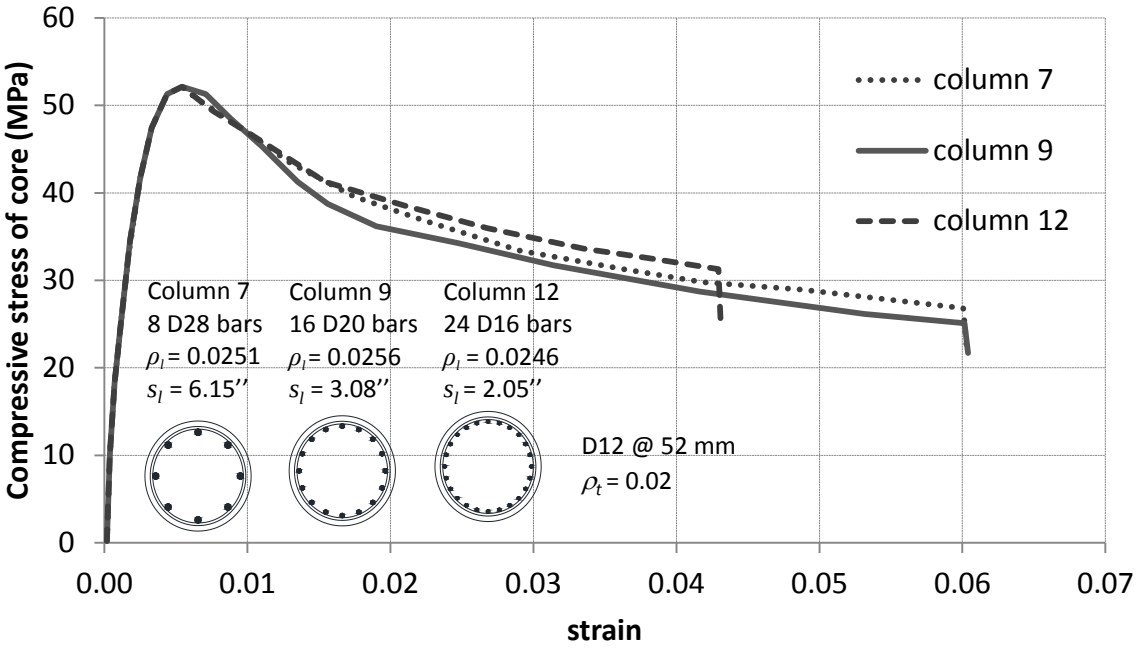

Figure 1.2 – Effect of spacing of longitudinal bars on circular columns (Mander et al. 1988b)

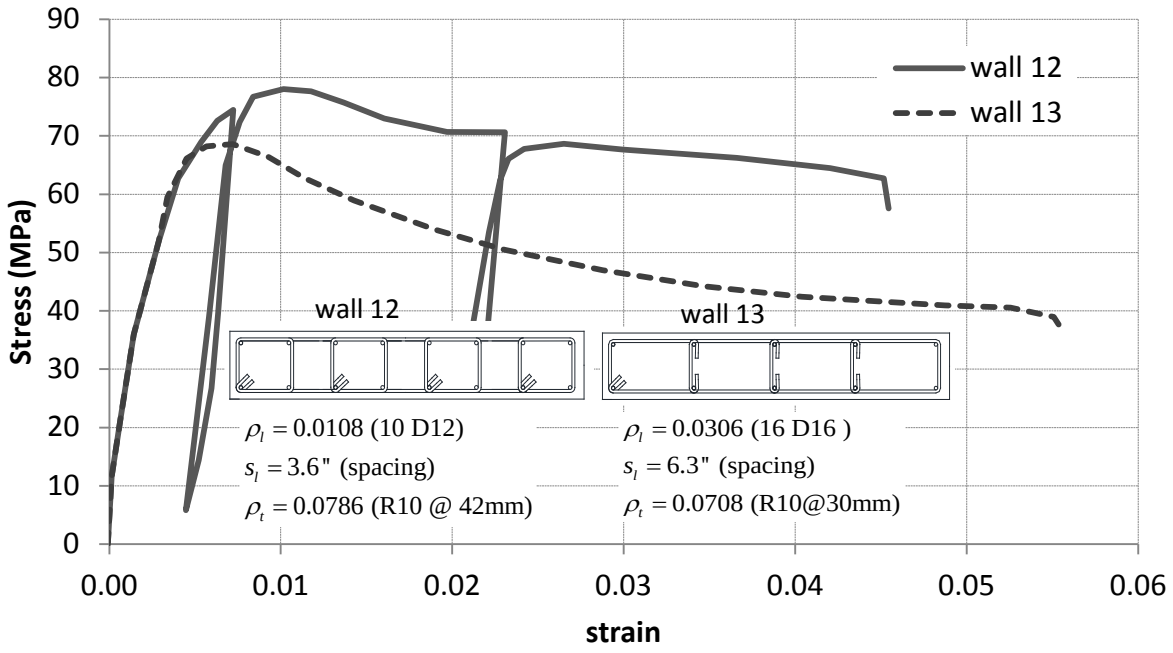

Figure 1.3 - Effect of spacing of longitudinal bars on rectangular sections (Mander et al. 1988b)

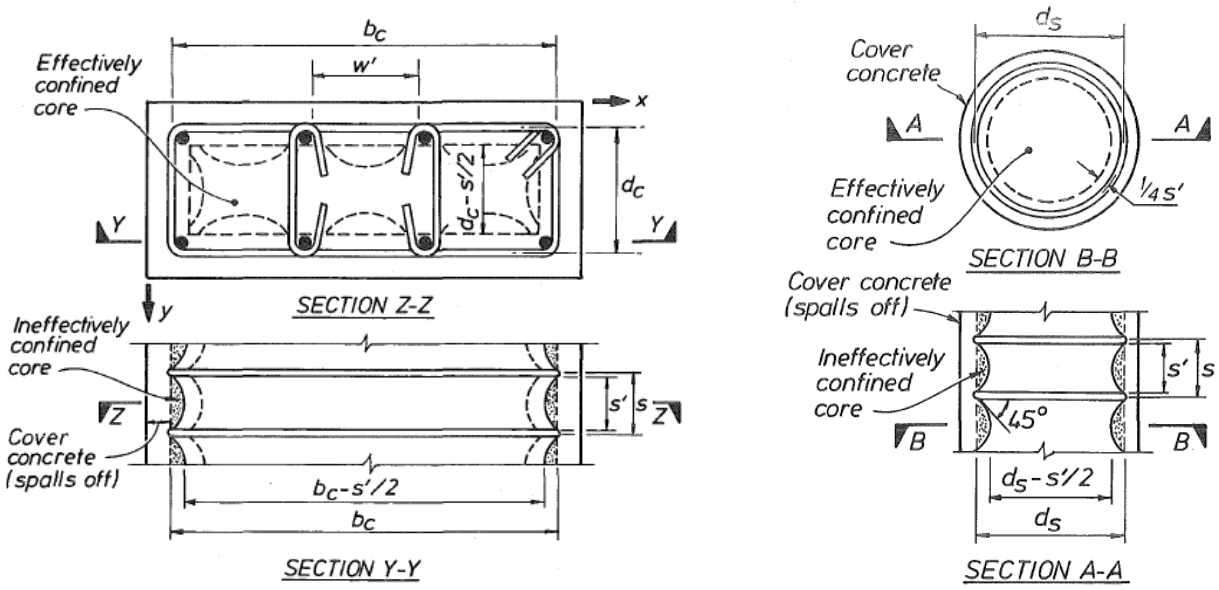

(a) Rectangular column (b) Circular column

Figure 1.4 – Arching action of confining reinforcement (Mander et al. 1988a)

2 Test program

The main objective of the test program was to investigate the influence of the spacing of longitudinal reinforcing bars on the structural performance of RC piles; and in particular, to examine the impact of having the bar spacing greater than 8 in., which is the maximum permitted by the Caltrans Bridge Design Specifications (BDS) (Caltrans 2003) and AASHTO LRFD Bridge Design Specifications (AASHTO 2010) for longitudinal bars in compression members. The test program consisted of two pile specimens. The specimens were designed according to the existing specifications of Caltrans and AASHTO except that one had the spacing of the longitudinal bars considerably greater than 8 in. while the other had the spacing less than 8 in. The performance of the specimens, in terms of their ductility under lateral loading, and crack spacing and widths, is examined and compared in the next chapter.

2.1 Test specimens

The specimens were tested as cantilever piles with a constant axial load. They had the same dimensions. The height of each pile was 10 ft. (from the base to the mid-height of the cap) and the diameter was 28 in.

The design and reinforcing details of the specimens are shown in Figure 2.1 through Figure 2.6 and summarized in Table 2.1. As shown in Figure 2.1 and the table, the two specimens had the same design with more or less the same amount of longitudinal reinforcement. The only difference between the two was the size and the spacing of the longitudinal bars. As shown in Figure 2.2, the longitudinal reinforcement of Specimen #1 consisted of 6 #11bars, which corresponds to a steel ratio of 1.52%. The center-to-center spacing of the bars was 11 in., violating the maximum limit of 8 in. permitted by the Caltrans and AASHTO LRFD specifications. In Specimen #2, the longitudinal reinforcement consisted of 10 #9 bars spaced at 6.75 in. on center, which corresponds to a steel ratio of 1.62%. The transverse reinforcement in both specimens consisted of #6 hoops spaced at 5.75 in. on center, which met the minimum clear spacing of 5 in. for reinforcing steel in piles according to Caltrans (2003) and AASHTO

(2010). The volumetric ratio of the transverse steel is 1.28%, which is only slightly less than the minimum (1.35%) required by Caltrans (2003) for compression members.

The concrete used for the pile specimens had a specified slump of 7 in. and a specified compressive strength of 4,500 psi with the maximum aggregate size of 3/8 in., conforming to concrete mixes typically used for cast-in-place drilled hole (CIDH) piles. Table 2.2 summarizes the mix design specified for the concrete. The expected compressive strength of the concrete at 28 days was 5,000 psi. The reinforcement used for the test program was Grade 60 steel conforming to ASTM A706/A706M-09b standards (ASTM 2009).

Table 2.1 - Reinforcement details of Specimens #1 and #2

Spec.	Pile Diameter D (in.)	Diameter of Confined Core* D_c (in.)	Long. Steel Ratio ρ_l	Long. Bars	Transverse Steel Ratio ρ_t	Angular Spacing of Long. Bars θ_l (deg.)	Linear Spacing of Long. Bars s_l (in.)
1	28	24	0.0152	6 #11	0.0128	60	11.04
2	28	24	0.0162	10 #9	0.0128	36	6.75

*Out-to-out diameter of hoops

Table 2.2 – Concrete Mix Design

Specified compressive strength = 4.5 ksi		
Material	Quantity (lbs/yd^3)	Proportion of Aggregate (%)
Cement	572.00	-
Flyash	143.00	-
Course aggregate	1455.00	51.88
Sand	1386.00	48.12
Water (w/c)	38.50 (0.45)	-
WRDA-64 (admixture)	18.00	-
ADVAHRWR (admixture)	43.00	-
Air content (%)	2.00	-

The footings and the caps of the pile specimens were designed with simple strut-and-tie models to ensure that no damage or major cracks would develop during the tests. Their design details are shown in Figure 2.3 through Figure 2.6. As shown in Figure 2.1, the spacing of the hoops inside the footings of the

specimens was reduced to 4 in. to provide adequate confinement for the development of #11 bars in Specimen #1. The same spacing was used for both specimens.

2.2 Test setup and procedure

The two pile specimens had the same test setup, which is shown in Figure 2.7 and Figure 2.8. They were tested as cantilever columns. The footing of each specimen was fixed onto the strong floor of the laboratory with 6 steel bars, each of which was post-tensioned to 200 kips. A constant axial load of 280 kips was applied on each specimen with a steel cross beam set on top of the pile cap, corresponding to 9% of the actual compressive strength of the specimens $\left(A_g f_c'\right)$. The steel beam was loaded by two steel rods that were post-tensioned with center-hole jacks located underneath the strong floor. Each specimen was loaded by one horizontal actuator with a load capacity of 220 kips and a total stroke of 48 in. One end of the actuator was attached to the reaction wall, while the other end was attached to the pile cap. The line of the horizontal load was 10 ft. above the base of the pile specimen. The specimens were subjected to cyclic lateral loading. A picture of the test setup is shown in Figure 2.9.

The loading history used in the tests is shown in the second column of Table 2.3. The lateral load-vs.-displacement curves for the two specimens were expected to be very similar, but Specimen #2 was expected to have a slightly higher lateral resistance not only because of the higher reinforcement ratio but also a higher proportion of the longitudinal bars in tension when the section was subjected to bending. To facilitate the comparison of the behaviors of the two specimens, it was decided that the same loading history be used in the two tests. The loading history was first determined for Specimen #1 with the help of a pre-test finite element analysis conducted on the specimen. In the first 4 cycles, the actuator was under force control, with the load increased in each cycle up to the level that corresponded to the first yield of the longitudinal reinforcement in Specimen #1 as predicted in the pre-test analysis. The specimen was then subjected to fully-reversed displacement-controlled load cycles with increasing ductility demands until the lateral load resistance dropped significantly due to the fracture of the longitudinal reinforcement.

Table 2.3 - Loading protocol for pile specimens

Cycle No.	Load/Displ. Amplitude (Same for both specimens)	Spec #1 (Δ_y=0.98") Actual Ductility Demand	Spec #2 (Δ_y=0.97") Actual Ductility Demand	Comment
1	±15 kips	-	-	25% of theoretical first yield
2	±30 kips	-	-	50% of theoretical first yield
3	±45 kips	-	-	75% of theoretical first yield
4	±60 kips	-	-	100% of theoretical first yield
5a, 5b	±1.2"	1.22	1.24	1% drift
6a, 6b	±2.4"	2.45	2.47	2% drift
7a, 7b	±3.6"	3.67	3.71	3% drift
8a, 8b	±4.8"	4.90	4.95	4% drift
9a, 9b	±7.2"	7.35	7.42	6% drift
10a, 10b	±9.6"	9.80	9.90	8% drift
11a, 11b	±12.0"	12.2	12.4	10% drift

The ductility demand on the pile specimens is defined as $\mu = \Delta / \Delta_y$, in which Δ is the lateral displacement at the level of the actuator, and Δ_y is the yield displacement of an equivalent elastic-perfectly plastic system as defined in Figure 2.10. As shown in the figure, Δ_y is the displacement at the intersection of the secant line passing through the original and the point $\left(\Delta_y', F_y'\right)$ with the horizontal line passing through the ultimate load F_y, i.e.,

$$\Delta_y = \frac{F_y}{F_y'}\Delta_y' \tag{0.1}$$

In the above expression, F_y' is the lateral load at which the first yield of the longitudinal bars occurs and Δ_y' is the corresponding displacement. The displacement amplitudes shown in the second column of

Table 2.3 were determined as an integer multiple of Δ_y that was calculated to be 1.2 in. with Equation 2.1 using the forces F_y' and F_y determined in the pre-test analysis and Δ_y' measured in the test, all for Specimen #1. However, the actual ductility demands and the values of Δ_y shown in the third and fourth columns of Table 2.3 are based on the actual values of F_y' and F_y obtained from the tests of the respective specimens. The maximum displacement applied in each test was 12 in., corresponding to 10% drift. The tests were stopped after a significant load drop had occurred due to the fracture of the longitudinal bars in the plastic-hinge zone near the base of the piles.

2.3 Instrumentation schemes

As shown in Figure 2.11 and Figure 2.12, each pile specimen was instrumented with displacement transducers along its height, an inclinometer at the mid-height of its cap, and strain gages on the longitudinal and lateral reinforcement. Transducers L48, L49, L50 and L51 were string potentiometers used to monitor the lateral deflection of each pile specimen at different elevations. Vertical linear potentiometers were mounted on the east and west faces of each pile specimen to measure the bending curvature developed along the height of the pile. Horizontal and diagonal linear potentiometers were mounted on the east face to measure shear deformation. Pictures of the west and east faces of the specimens are shown on Figure 2.13 and Figure 2.14, respectively.

Strain gages were attached onto the longitudinal reinforcement in positions close to the base of the pile specimens, as shown in Figure 2.15, to measure strains in the plastic-hinge zone, and in the footings to measure strain penetration. At elevations adjacent to the base of a pile, two strain gages were attached at each location on opposite sides of a reinforcing bar so that bending strains (due to bar buckling for example) could be identified and separated from the axial strain. The transverse reinforcement near the base of a pile also had strain gages, as shown in Figure 2.16. A picture of strain gages attached to the reinforcement of Specimen #1 is shown in Figure 2.17.

2.4 Specimen construction and material properties

The two pile specimens were constructed at the same time by an outside contractor. Each specimen was cast in two phases. First, the reinforcement cages were assembled and the forms for the footings were fabricated. The footings were cast first. Thirty days later, the piles and the caps were cast. The time separation between these two concrete placements was decided according to the test dates scheduled for the two specimens in order that the age of the concrete in the piles would not significantly exceed 28 days and the compressive strength would be close to 5,000 psi. The forms for the footings and the piles were removed about one week after the casting of the piles. The steel cages of the pile specimens before casting are shown in Figure 2.18 and Figure 2.19. During the concrete placements, six-inch-diameter concrete cylinders were prepared for compression and split-cylinder tests. Compression tests were conducted during the curing of the pile specimens to determine whether the targeted concrete strength of 5,000 psi had been reached. Compression and split-cylinder tests were conducted on the day of each pile test. Table 2.4 shows the average uniaxial compressive strengths and split-cylinder strengths of the concrete in the pile specimens on the day of structural testing. The stress-strain curves for the reinforcing bars were obtained by tension tests. Three bars were tested for each bar size. The average yield and ultimate strengths of the bars are shown in Table 2.5, while the stress-strain curves are shown in Figure 2.20 through Figure 2.22.

Table 2.4 - Uniaxial compressive strengths of concrete

Concrete	Date cast	Date tested	Days after casting	f_c' (ksi)	f_t' (ksi)*
Spec #1 pile	June 12, 2012	July 12, 2012	30	4.9	0.40
Spec #1 footing	March 8, 2012	July 12, 2012	157	7.4	-
Spec #2 pile	June 12, 2012	July 17, 2012	35	5.2	0.37
Spec #2 footing	March 8, 2012	July 17, 2012	162	7.5	-

*****Split-cylinder strength

Table 2.5 – Reinforcement properties

	#6 (hoops)	#9 (long.)	#11 (long.)
Yield (ksi)	-	67	64
Ultimate (ksi)	95	96	90

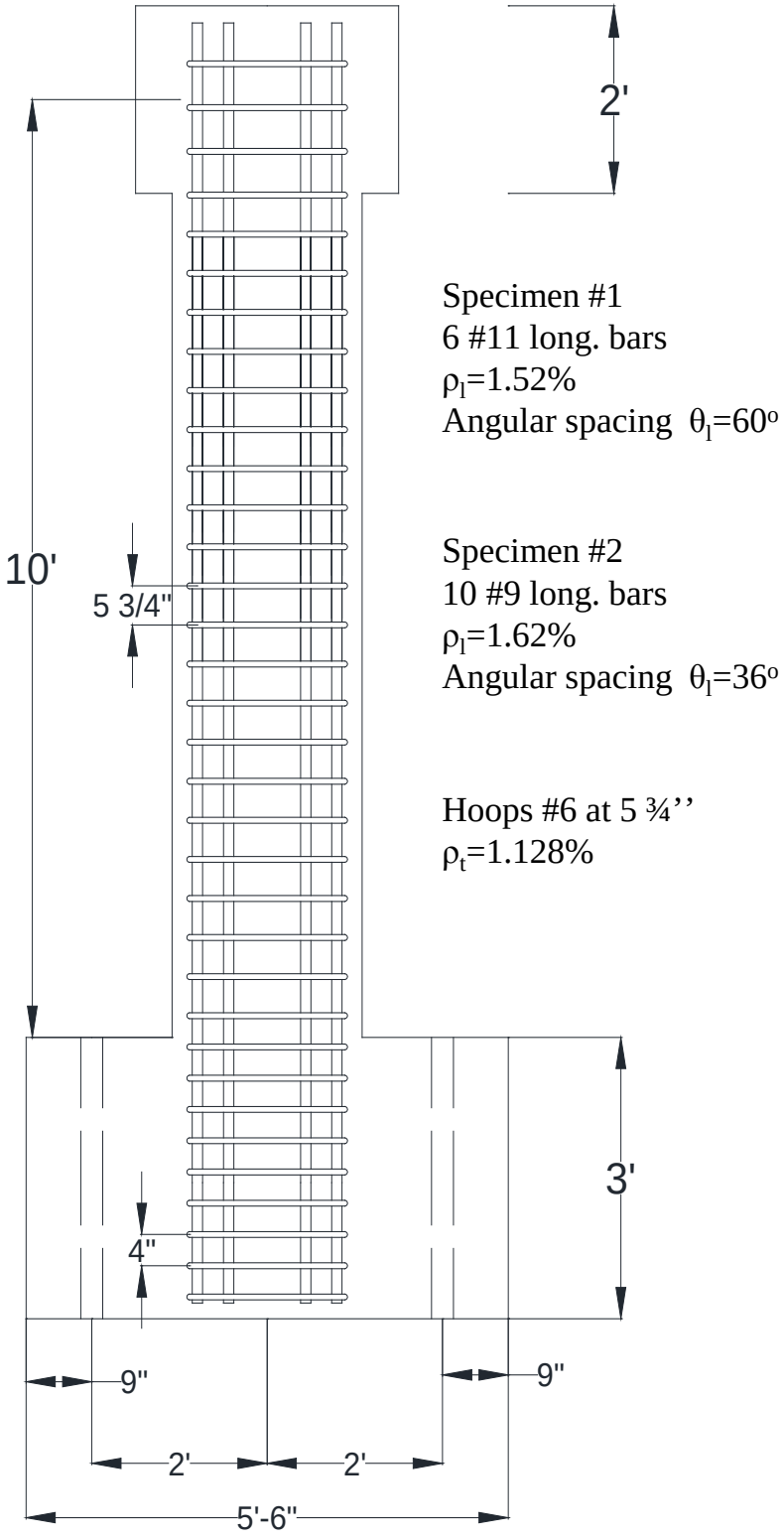

Figure 2.1 - Elevation view of Specimens #1 and #2

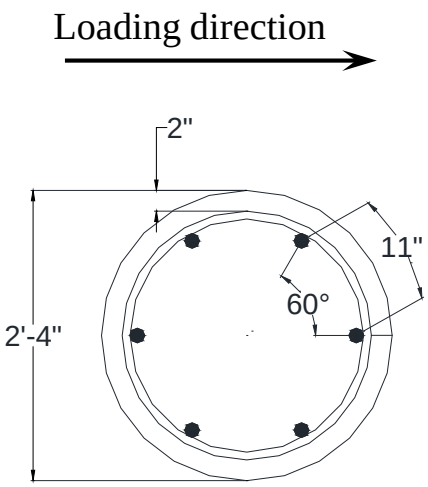

Specimen #1
6 #11 long. bars
ρ_l=1.52%

Confining hoops
#6 at 5 ¾’’
ρ_t=1.28%

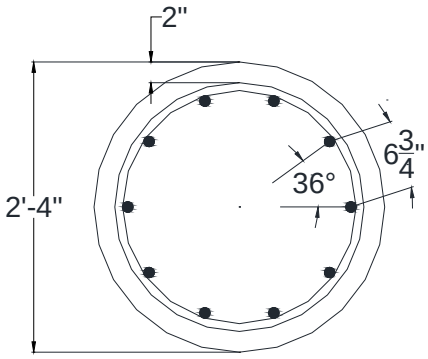

Specimen #2
10 #9 long. bars
ρ_l=1.62%

Confining hoops
#6 at 5 ¾’’
ρ_t=1.28%

Figure 2.2 – Cross-sections of Specimens #1 and #2

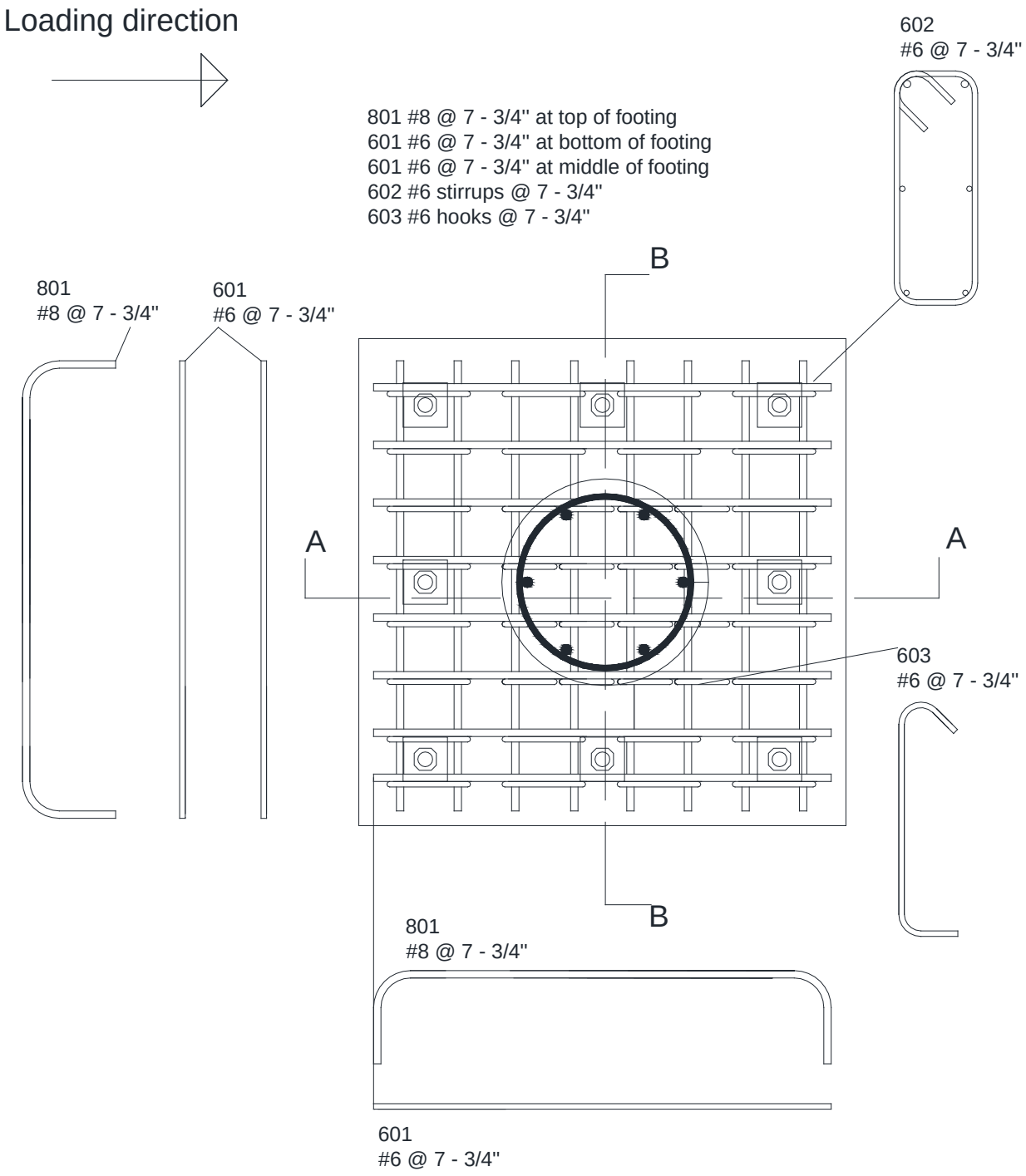

Figure 2.3- Plan view of footing details

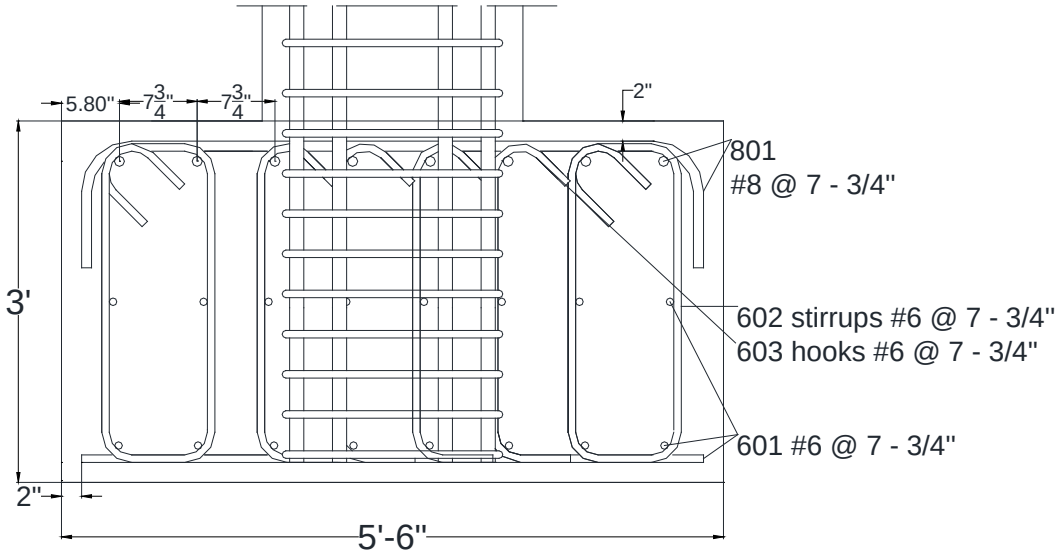

Section A-A

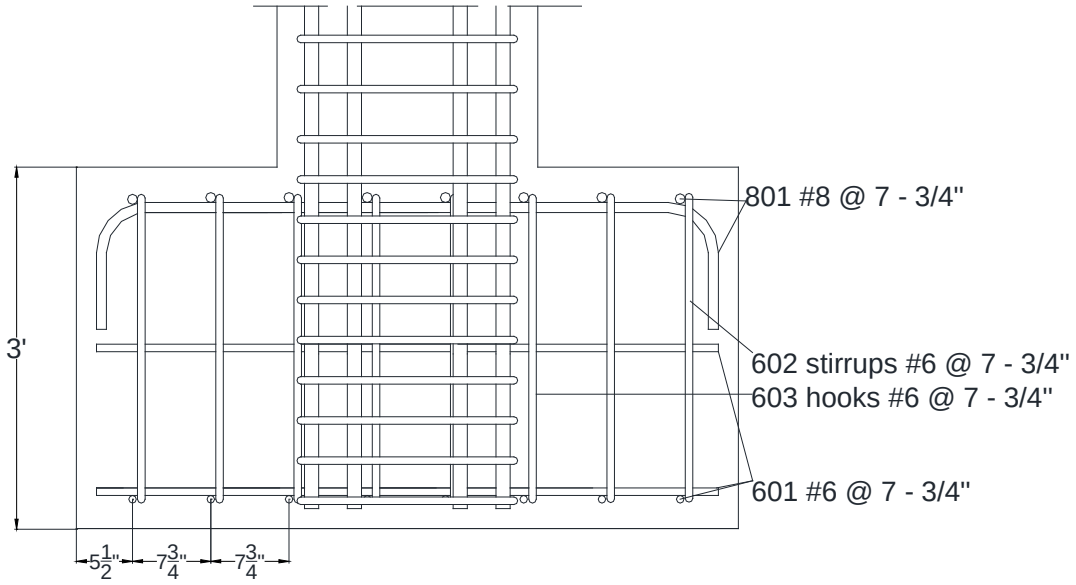

Section B-B

Figure 2.4 – Elevation view of footing details (see Figure 2.3 for section locations)

z

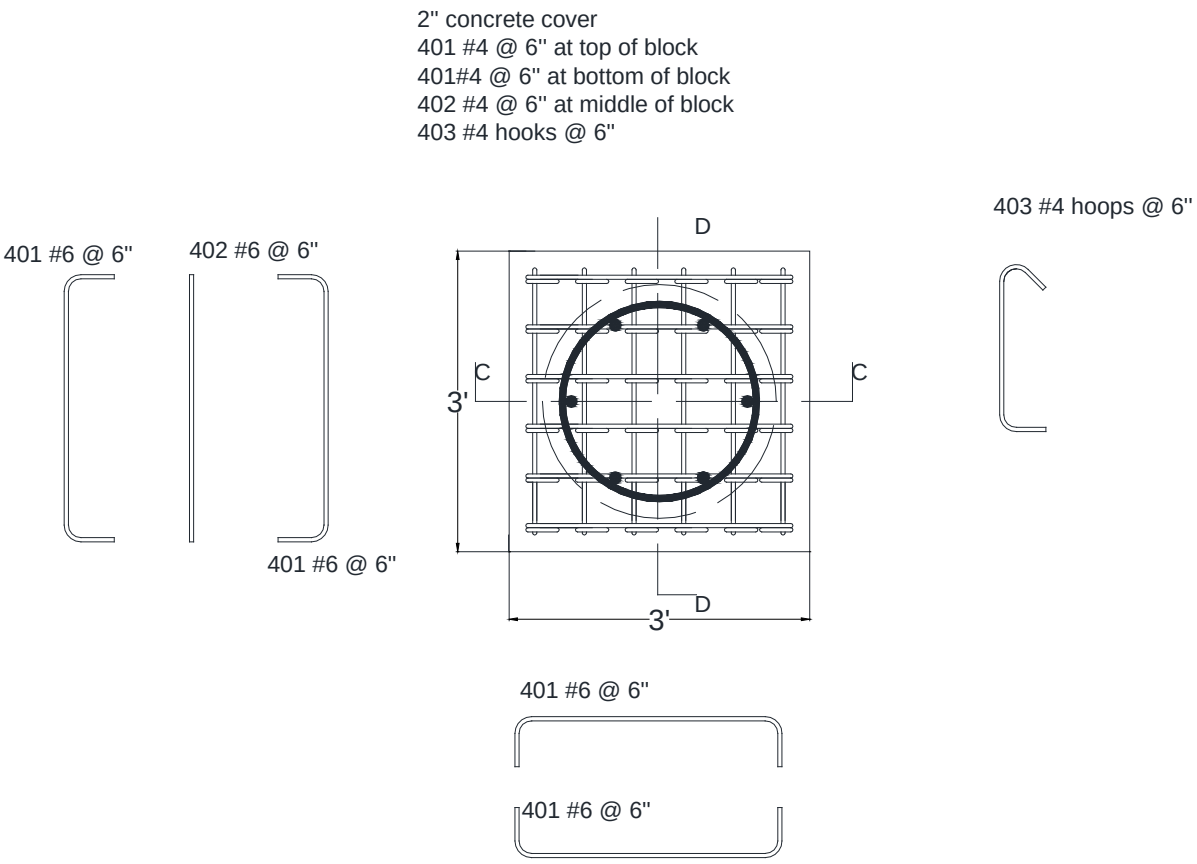

Figure 2.5 – Plan View of cap details

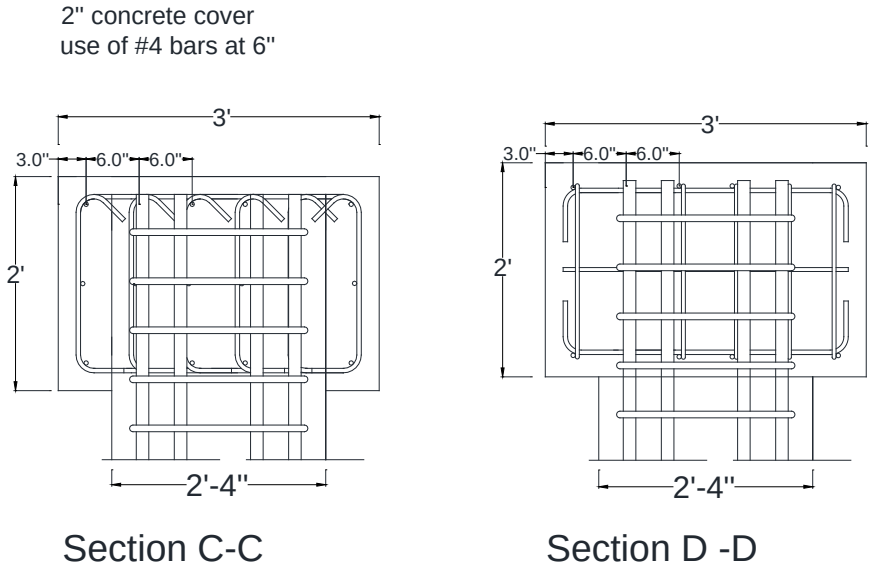

Figure 2.6 – Elevation view of cap details (see Figure 2.5 for section locations)

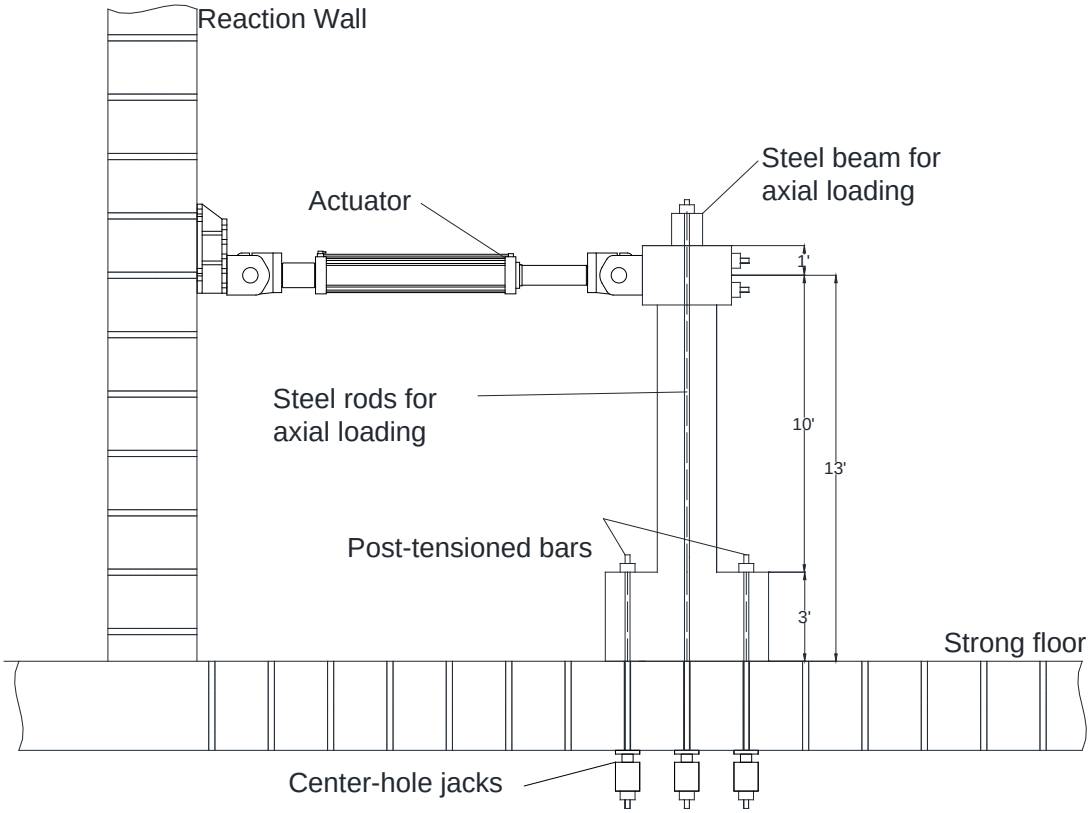

Figure 2.7 - Elevation view of test setup

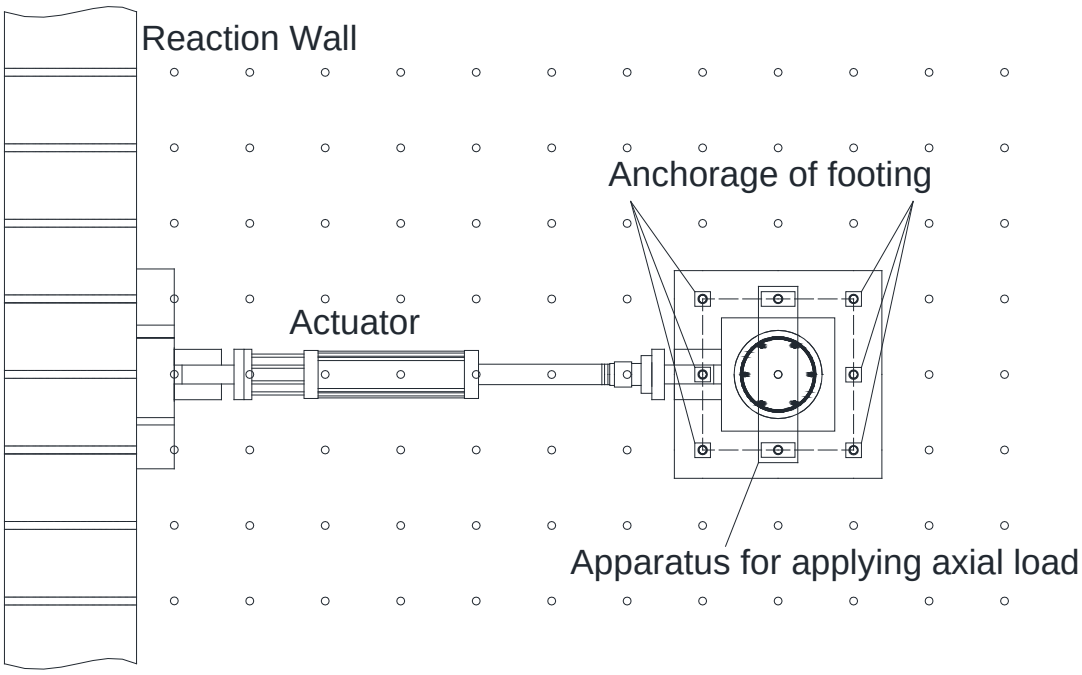

Figure 2.8 - Plan view of test setup

Figure 2.9 Picture of Specimen #1 test setup

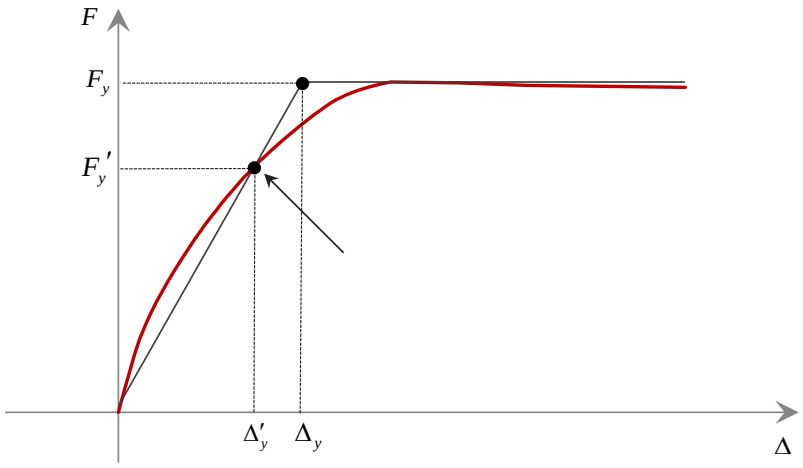

Figure 2.10 – Equivalent elastic-perfectly plastic system

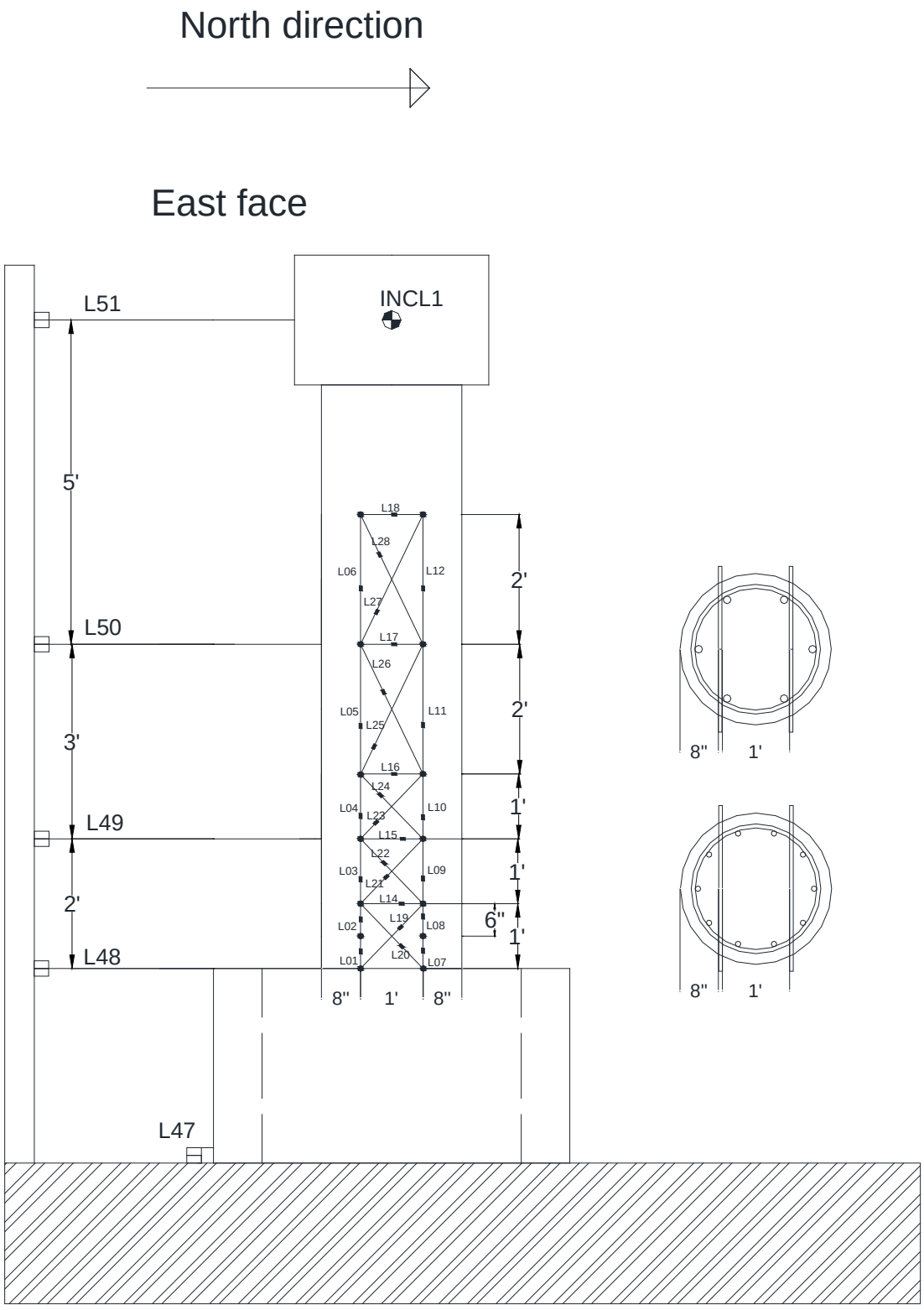

Figure 2.11 - Elevation view of displacement transducers (East face)

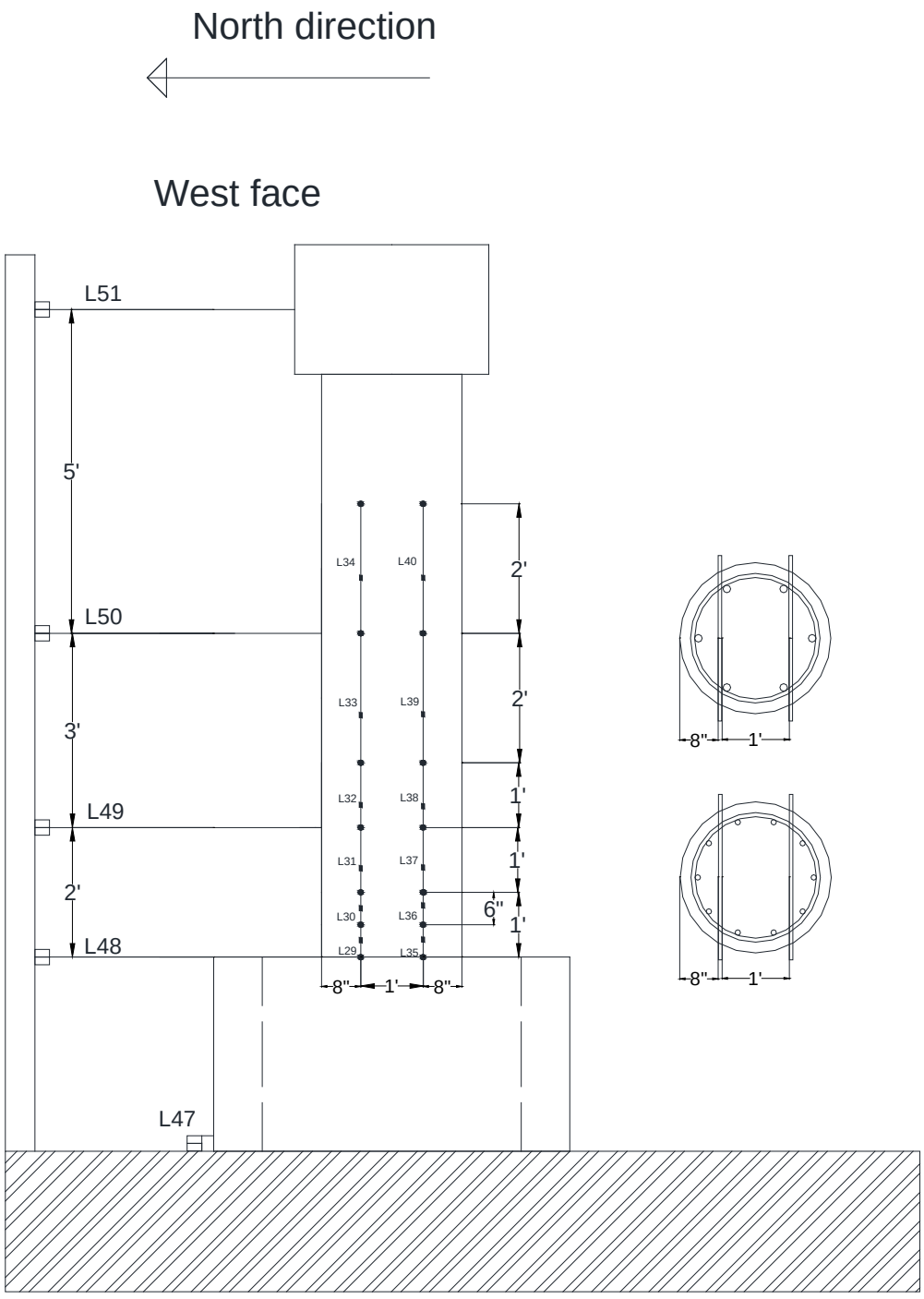

Figure 2.12 - Elevation view of displacement transducers (West face)

Figure 2.13 - Picture of displacement transducers mounted on west face of Specimen #1

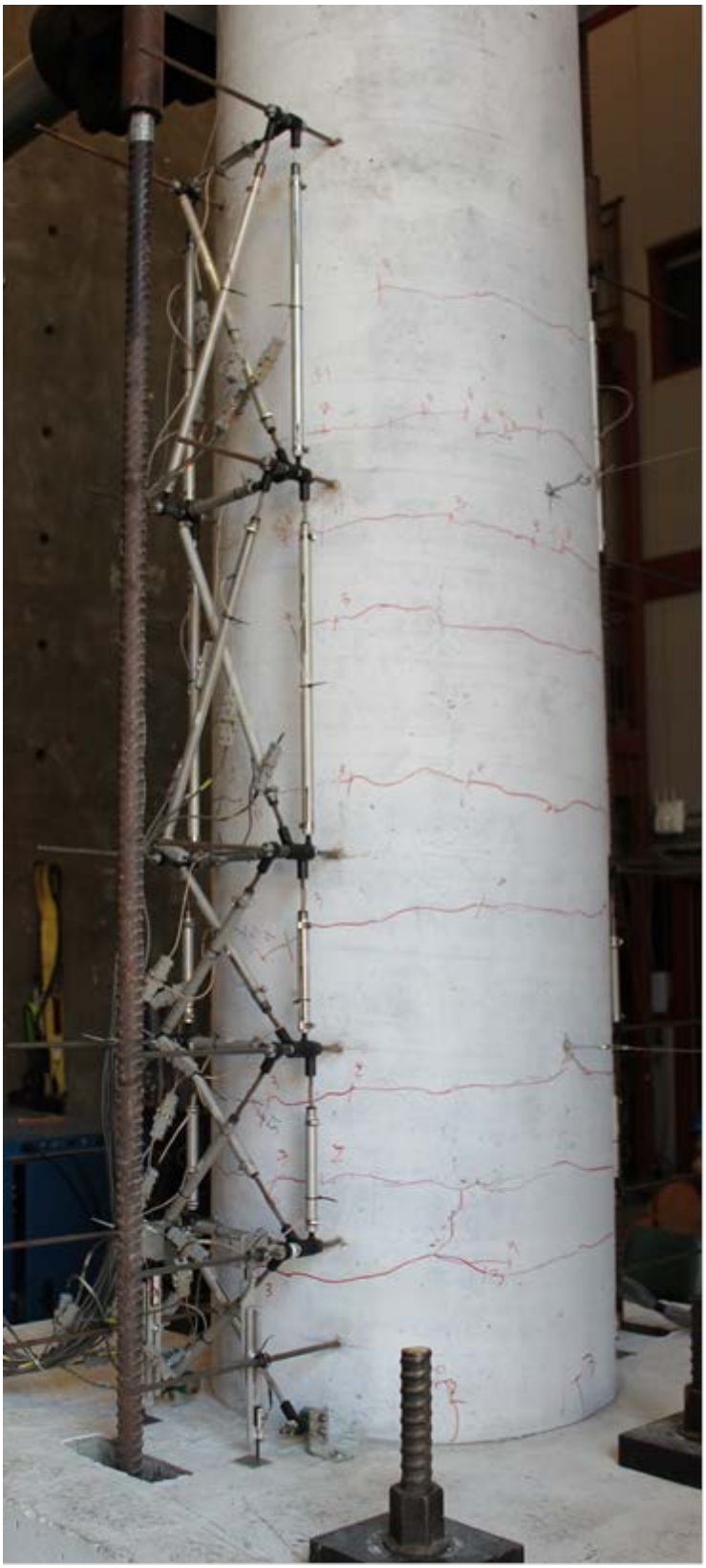

Figure 2.14 – Picture of displacement transducers mounted on east face of Specimen #2

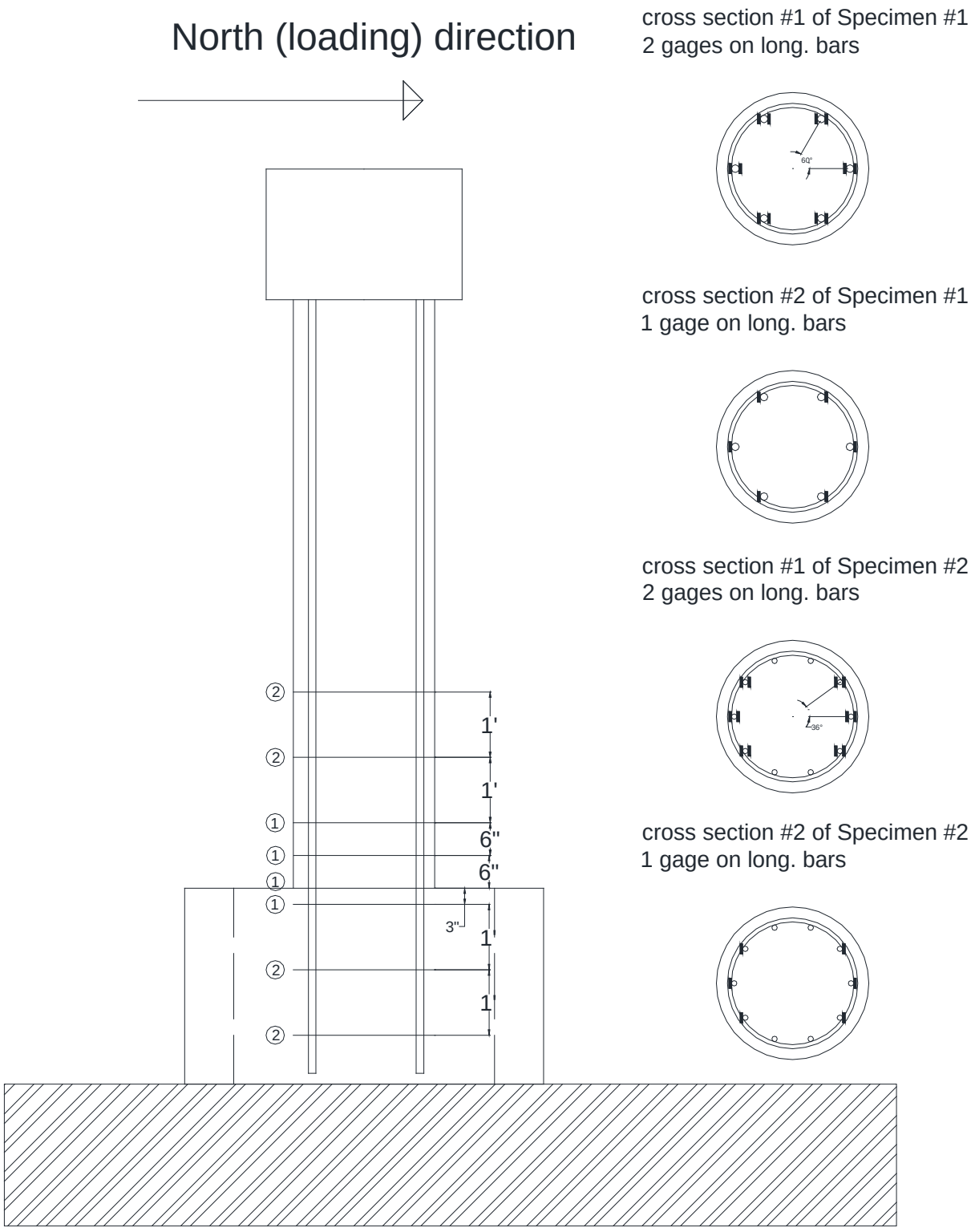

Figure 2.15 - Strain gages on longitudinal bars of Specimens #1 and #2

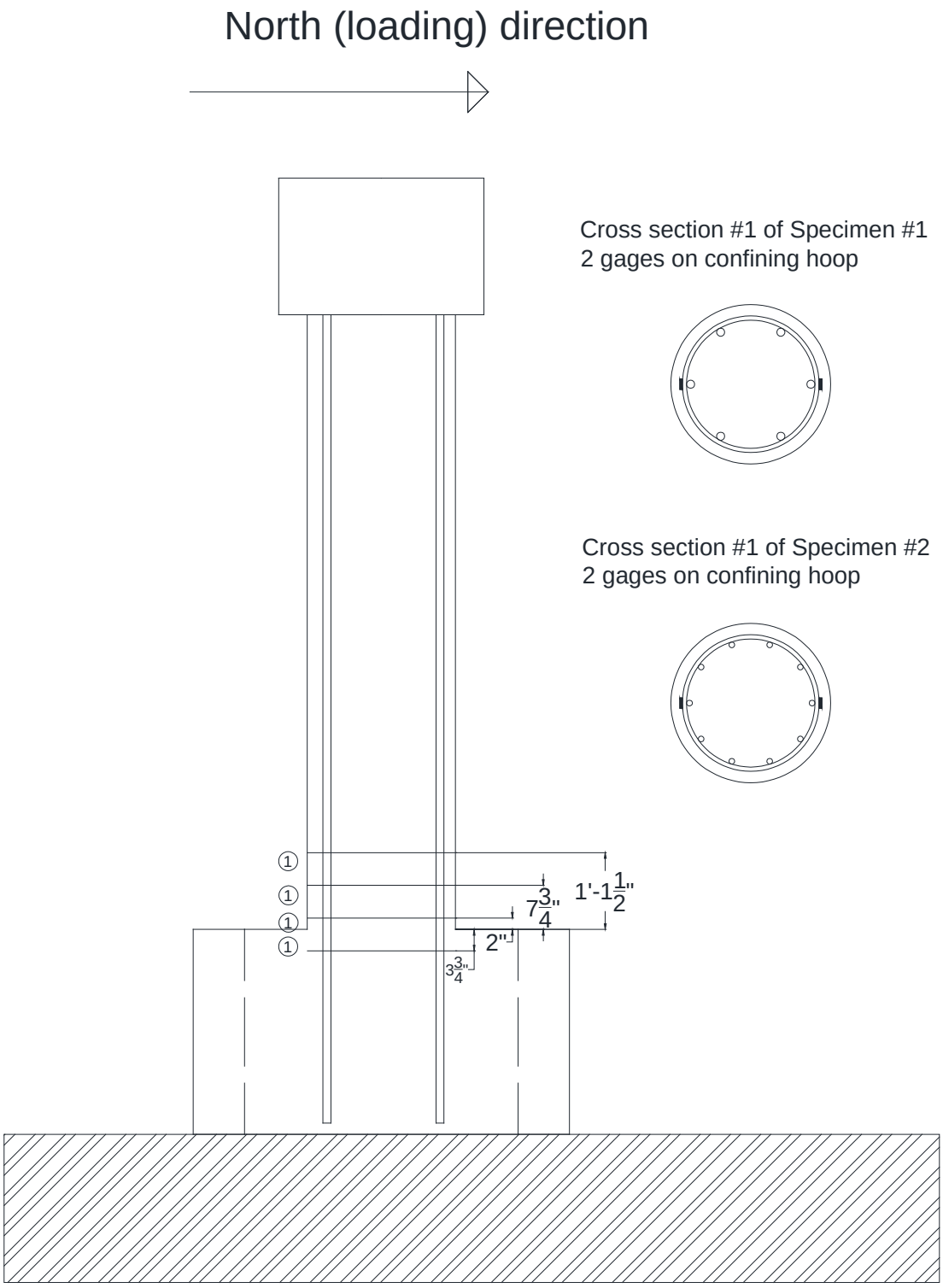

Figure 2.16 - Strain gages on steel hoops of Specimens #1 and #2

Figure 2.17 – Picture of strain gages on reinforcing bars of Specimen #1

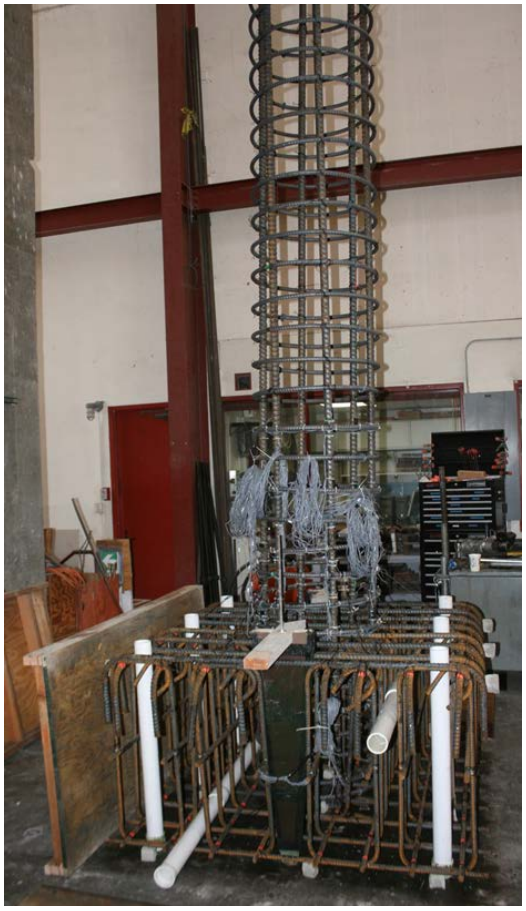

Figure 2.18 - Reinforcement cage for Specimen #1

Figure 2.19 - Assembled forms for casting of footings

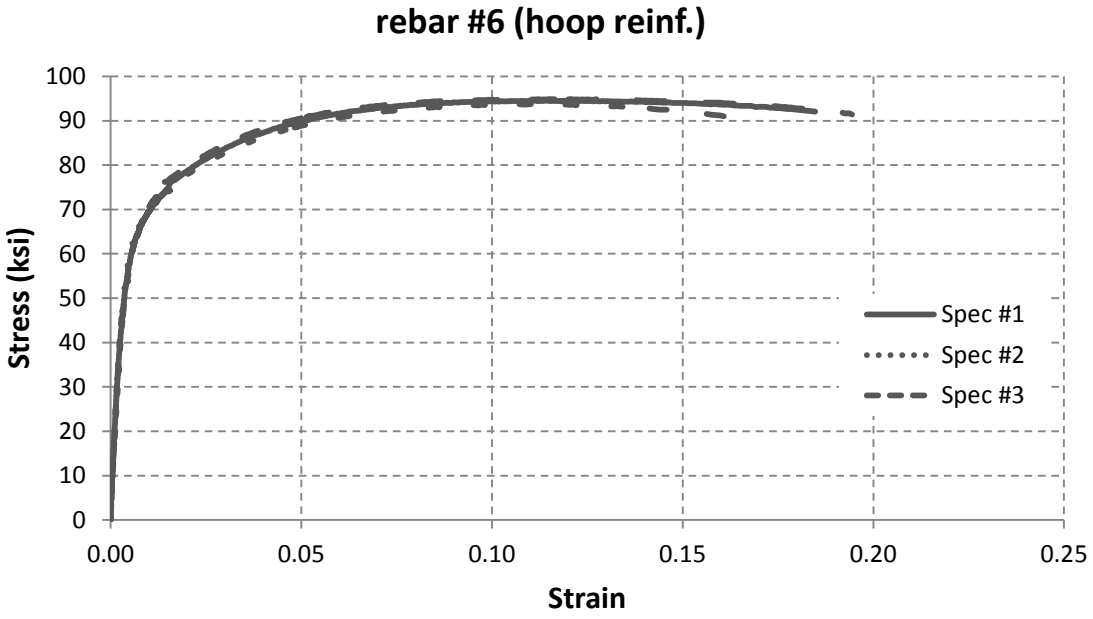

Figure 2.20 – Stress – strain curves for #6 hoop reinforcement

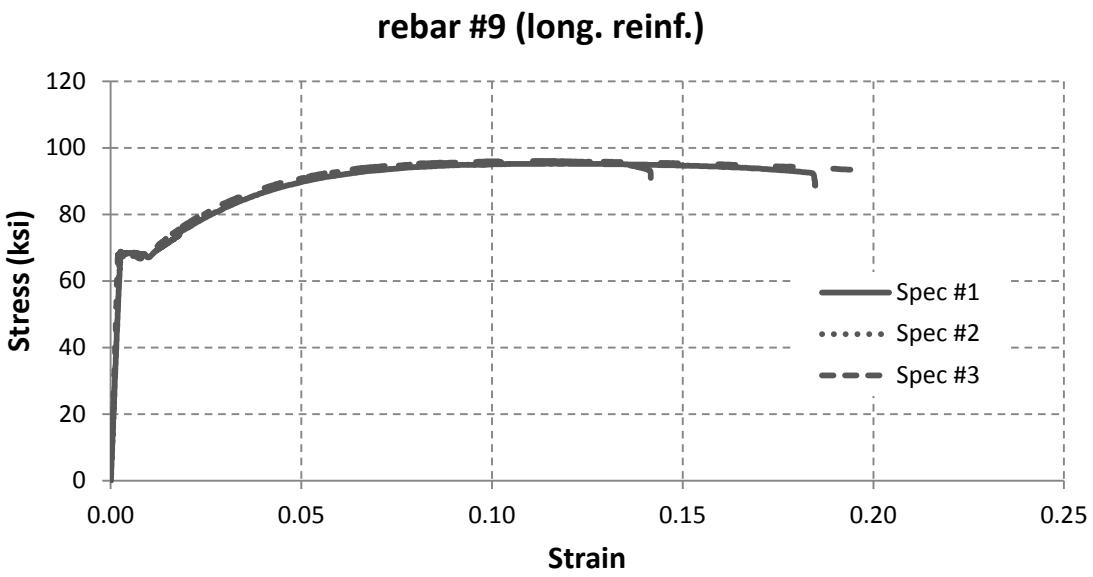

Figure 2.21 - Stress – strain curves for #9 longitudinal reinforcement

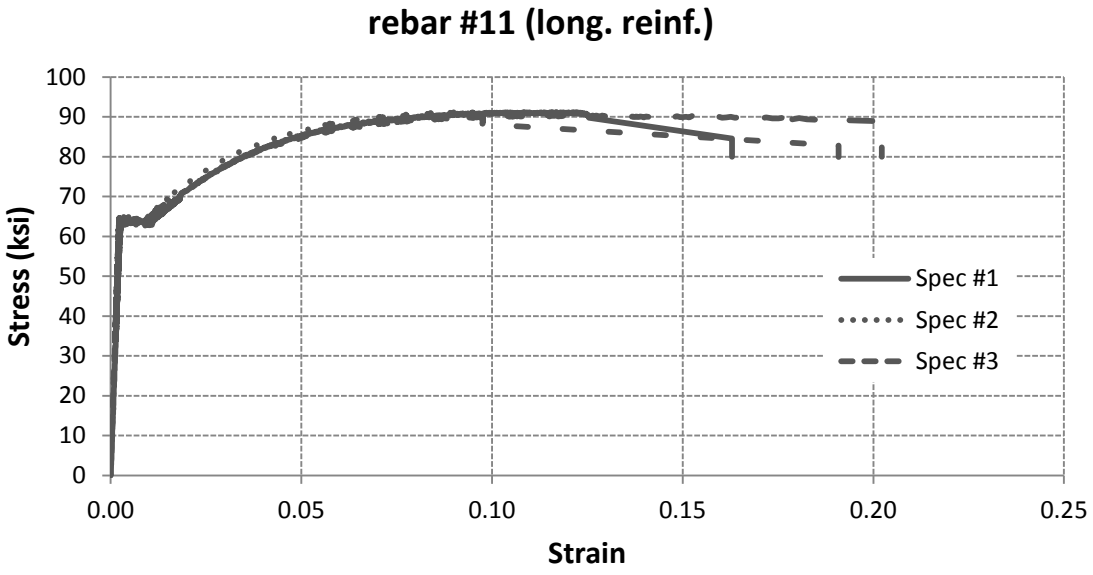

Figure 2.22 – Stress - strain curves for #11 longitudinal reinforcement

3 Test results

This chapter presents the test results obtained from pile Specimens #1 and #2. Both specimens had the same dimensions. The first specimen had 6 #11 longitudinal reinforcing bars and the second had 10 #9 bars. For each of these specimens, the main test observations, load-vs.-displacement relations, curvature distributions along the pile, and strains in the reinforcement are presented and discussed.

3.1 Overall behavior of Specimen #1

The lateral load-vs.-lateral drift ratio for Specimen #1 is shown in Figure 3.1. The lateral displacement is obtained by transducer L51 as shown in Figure 2.11. The dashed curve shows the total lateral force applied by the actuator, while the solid curve shows the corrected lateral force, which takes into account the large displacement effect of the post-tensioned rods that exerted the vertical load. The corrected force is obtained by subtracting the horizontal component of the total force exerted by the post-tensioned rods from the actuator force. Figure 3.2 shows the variation of the total force exerted by the rods as the drift of the pile increased. It can be seen that the force varied between 270 and 300 kips while the target value was 280 kips. As shown in Figure 3.1, Specimen #1 had a lateral load capacity of 69 kips, which was reached at a drift ratio of 1.7%. After the maximum lateral resistance had been reached, the peak resistance attained in the subsequent cycle shows a significant decrease as compared to that in the previous. This was caused by the compressive failure of the concrete cover at the compression toe of the pile specimen. The corrected lateral load-vs.-drift curve shows a mild gradual decrease of the lateral resistance with increasing drift due to the *P-Δ* effect. Buckling of bar #1, which was near the south face of the pile as shown in Figure 3.1, was observed in the 2nd cycle at -8% drift, corresponding to a ductility demand of 9.8. During the 1st cycle at +10%, bar #4, which was near north face, buckled. In the 2nd cycle at +10% drift, bar #1 fractured in tension, resulting a sharp drop in the resistance of the pile. In the subsequent unloading and reloading to the other direction, bar #4 fractured. Figure 3.3 shows a plot of the moment resistance of the cross-section at an elevation of 0.5 ft. from the base against the average

curvature measured over a distance of 1 ft. from the base of the pile specimen. The calculation of the applied moment includes the lateral load and the *P-Δ* effect of the vertical load. The moment-curvature relation shows a very ductile behavior with little decrease in the moment resistance as the curvature increased till bar fracture occurred.

Flexural cracking in concrete initiated in the 1st force-controlled cycle. The horizontal cracks around the circumference of the pile propagated from cycle to cycle quite rapidly. At 1% drift, corresponding to a ductility demand of 1.22, flexural cracks developed over a height of 5 ft. with more or less uniform spacing of 9 to 12 in. as shown in Figure 3.4. At a drift of 2%, concrete cover near the base of the pile started to show compressive damage with visible vertical cracks, as shown in Figure 3.5. At this drift level, widely opened flexural cracks were observed. Figure 3.6 shows the spalling of the concrete cover near the base of the pile specimen at 3% drift. In this cycle, a peak load of 10 kips was reached, which is lower than that in the previous cycle of 2% drift as shown in Figure 3.1. This was probably caused by the spalling of the concrete as noted above. At this drift level, the width of the flexural cracks was more than ¼ in. as shown in Figure 3.6.

As shown in Figure 3.7, at 6% drift, concrete spalling was deeper into the pile and extended from the base of the pile up to a height of 1.5 ft. Moreover, a longitudinal reinforcing bar and part of the horizontal hoops were exposed due to the concrete spalling. In the 2nd cycle of -8% drift, corresponding to a ductility demand of 9.8, bar #1 at the south face buckled, as shown in Figure 3.8. During the 1st cycle of -10% drift, the buckling of bar #1 became quite severe, as shown in Figure 3.9a. Figure 3.9b shows the bending deformation observed in bar #4 at the north face during the 1st cycle of +10% drift. Both bars bent outward between two adjacent hoops. Concrete spalling extended up to a height of 2 ft. from the base of the specimen exposing the longitudinal bars and the hoops. Parts of the confined core was crushed as shown in Figure 3.9.

During the 2nd cycle of +10% drift, buckled bar #1 at the south face fractured in tension (Figure 3.10a), while bar #4 at the north face had severe buckling (Figure 3.10b). During the load reversal, buckled bar #4 at the north face also fractured in tension as shown in Figure 3.11. At that point, the test was

terminated and the top of the specimen was brought back to zero lateral displacement. A drift of 10% corresponds to a lateral displacement of 12 in. Figure 3.12 shows pictures of Specimen #1 at the end of the test, zooming-in on the two bars that fractured, with one at each face of the pile, and the severe crushing of the concrete. The section at 10 in. above the base of the pile had the most severe damage.

3.2 Overall behavior of Specimen #2

Figure 3.13 shows the lateral load-vs.-drift curves of Specimen #2, which had 10 #9 longitudinal bars. The corrected lateral load-vs.-drift ratio curve is derived in the same way as that for Specimen #1. Figure 3.14 shows the variation of the total force exerted by the post-tensioned rods with drift. Pile Specimen #2 had a maximum load capacity of 78 kips, which was reached at a drift of 1.6%. The drop of the load resistance of Specimen #2 due to the P-Δ effect is clearly shown.

During the 1st cycle of +8% drift, corresponding to a ductility demand of 9.9, bar #4 placed at the north face started to buckle. During the load reversal at -8% drift, bar #1 at the south face buckled. In the 2nd cycle of +8% drift, bar # 4 at the north face had severe buckling. During the reversal to -8% drift, bar #2 at the south face also buckled, while the bending deformation of bar #1 was quite large. During the 1st cycle of +10% drift, bar #1 fractured in tension, while bars #3, #4 and #5, which were in compression, buckled. In the following displacement reversal, bars #4 and #5 at the north face fractured in tension, resulting in sharp drops in the lateral load resistance as shown in Figure 3.13. Figure 3.15 shows the moment resistance plotted against the average curvature measured over a distance of 1 ft. from the base of the pile specimen. Similar to that for Specimen #1, the moment-curvature relation shows a very ductile behavior till bar fracture occurred.

For Specimen #2, flexural cracking in concrete initiated in the 2nd force-controlled cycle, one cycle later as compared to Specimen #1. At 1% drift, corresponding to a ductility demand of 1.24, flexural cracks spaced at 6 to 9 in. developed over a height of 6 ft., as shown in Figure 3.16. Figure 3.17 shows the bottom portion of Specimen #2 at the drift of 2% where the concrete cover had multiple vertical cracks

indicating the initiation of toe crushing. The flexural cracks in Specimen #2 were more closely spaced than those in Specimen #1, and their spreading from cycle to cycle was slower.

As shown in Figure 3.18, at 3% drift, the spalling of the concrete cover extended up to 2.5 ft. from the base. In this cycle, the peak load had a significant drop as compared to that in the previous cycle, as Figure 3.13 shows. The flexural cracks developed in the pile were quite wide with a width of about 0.25 in. At 4% drift, the extent of the spalling of the concrete cover remained at 2.5 ft. as shown in Figure 3.19. As shown in Figure 3.20, at 6% drift, the spalling of the concrete cover near the base was severe, exposing parts of the transverse and longitudinal reinforcement on the south and north faces. The spalling of the concrete cover extended up to a height of about 3 ft. from the base of the pile, which is more extensive than that in Specimen #1 at the same drift level.

During the 1st cycle of +8% drift, bar #4 at the north face had some bending deformation, as shown in Figure 3.21b. During the subsequent displacement reversal at -8% drift, bar #1 at the south face buckled, as shown in Figure 3.21a. Figure 3.22a shows buckled bars #1 and #6 at the south face of Specimen #2 during the 2nd cycle of -8% drift. Figure 3.22b shows the north face of Specimen #2 where bar #4 bent in a plane that was tangential to the circumference of the pile. Crushing of the concrete core was also observed around the region where the longitudinal bars buckled.

At the beginning of the 1st cycle of +10% drift, buckled bar #1 at the south face fractured in tension, while bars #4 and #5 at the north face, which were in compression, had severe buckling, as shown in Figure 3.23. In the following displacement reversal at -10% drift, buckled bars #4 and #5 at the north face fractured in tension as shown in Figure 3.24. At that point, with the fracture of bars #1, #4, #5, and the buckling of bars #2 and #6, the test was terminated. The maximum drift of 8% reached before the fracture of the longitudinal bars corresponds to a lateral displacement of 9.3 in. Figure 3.25 shows pictures of Specimen #2 at the end of the test. The section at 12 in. above the base of Specimen #2 had the most severe crushing of the concrete core.

3.3 Comparison of specimen behaviors

3.3.1 Load – displacement response

The lateral load-vs.-drift behaviors of the two specimens are very similar. The two specimens had the same dimensions, almost the same quantities of reinforcement, and similar material properties. The lateral load capacity of Specimen #2 was 78 kips, which is 9 kips higher than that of Specimen #1. The higher load capacity of Specimen #2 can be attributed to the slightly higher quantity of the longitudinal reinforcement and also to a higher proportion of the longitudinal bars in tension when the section was subjected to bending.

The normalized lateral force-vs.-drift curves for Specimens #1 and #2 are compared in Figure 3.26. It can be seen that Specimens #1 and #2 had similar responses up to 8% drift. After that, Specimen #2 had load degradation started earlier than Specimen #1 due to the fracture of longitudinal bars. For Specimen #2, the fracture of longitudinal bars occurred during the 1^{st} cycle of 10% drift, while for Specimen #1, bar fracture occurred in the 2^{nd} cycle of 10% drift. This is because bar fracture was largely caused by the severe bending strain induced by buckling and Specimen #1 had #11 bars, which had a better resistance against buckling than the #9 bars in Specimen #2 given the same hoop spacing in the two specimens.

For both specimens, the gradual decrease of the lateral load resistance with increasing drift was mainly caused by the *P-Δ* effect. The above conclusion is supported by the fact that this gradual drop in resistance is not observed in the moment-curvature relations measured near the base of the two specimens, as shown in Figure 3.27. As shown, the moment resistances were more or less maintained with very mild decrease as the curvatures increased until the buckled bars fractured in tension. Specimens #1 and #2 had the same quantities of confinement steel, which were #6 hoops spaced at 5.75 in. on center, complying with the Caltrans BDS (Caltrans 2003) and the AASHTO LRFD BDS (AASHTO 2010). With this confinement level, the pile sections showed a very ductile behavior.

Moreover, Figure 3.27 shows that Specimen #1 developed a larger curvature near the base than Specimen #2, while the drift levels reached in the two specimens are not so different. This is consistent with the

observation that the plastic deformation (i.e., the bar yielding and concrete crushing) observed in Specimen #1 was more localized at the bottom of the pile than that in Specimen #2, resulting in a higher curvature demand in Specimen #1.

3.3.2 Crack patterns

The tests have shown a clear influence of the spacing and the size of the longitudinal reinforcement on the spacing and the width of the horizontal flexural cracks, which is a well-known fact. As shown in Figure 3.4 and Figure 3.16, flexural cracks were more widely spaced in Specimen #1 than in Specimen #2. Distances of flexural cracks in Specimen #1 were 6 to 9 in., while those in Specimen #2 were 9 to 12 in. Moreover, the width of the flexural cracks in Specimen #1 was also larger as shown in Figure 3.6 and Figure 3.18.

3.3.3 Curvature distributions

Curvature distributions along the height of Specimens #1 and #2 are shown in Figure 3.28 and Figure 3.29, respectively. The curvature was calculated with the readings from the vertical transducers mounted on the pile specimens, namely, L01 to L12 on the east face and L29 to L40 on the west face of each pile specimen, as shown in Figure 2.11 and Figure 2.12. As shown, the curvature distributions are consistent with the extent of concrete spalling observed in the two specimens (see Figure 3.12 and Figure 3.25). Specimen #1 had both the concrete spalling and plastic curvature more localized near the base, while those of Specimen #2 were distributed along a greater distance. As noted before, Specimen #1 had also the horizontal flexural cracks spaced farther apart due to the larger spacing and larger diameter of the longitudinal bars. Whether the difference in curvature distributions in the two specimens is related to the size and spacing of the bars or crack spacing requires further studies. However, this could be related to the higher tensile stresses developed in the longitudinal bars in Specimen #2 as discussed below.

3.3.4 Strain distributions in longitudinal reinforcement

Figure 3.30 through Figure 3.35 show the strains in the longitudinal bars of Specimens #1 and #2 at different drift levels. At large drifts, some of the bars buckled at an elevation of 12 in. from the base.

Within this region, two gages were mounted at each location on the diagonally opposite sides of a bar. To take out the influence of bar bending, values obtained from these pairs of gages are averaged.

Figure 3.30 shows that at a drift of 1%, the maximum tensile strain in the longitudinal bars at the base of Specimen #1 slightly exceeded the yield strain of 0.0023, while Figure 3.31 shows that for Specimen #2, the maximum tensile strain in the bars slightly exceeded 0.01 at +1% drift. Figure 3.32 and Figure 3.33 show the strains in the bars in Specimens #1 and #2 at a drift of 4%. The maximum tensile strains measured were between 0.02 and 0.04. For drift ratios between 6% and 8%, many of the gages were damaged and the maximum tensile strains measured were between 0.04 and 0.05. The higher tensile strains attained in Specimen #2 can be attributed to the smaller diameter of the longitudinal bars, which had less bond demand and therefore less slip and more concentrated plastic deformation in the vicinity of a crack. The higher tensile strains resulted in higher tensile stresses in the longitudinal bars, which could have led to more a more uniform curvature distribution in Specimen #2 as noted in the previous section. Furthermore, the #9 bars in Specimen #2 had higher yield and tensile strengths that the #11 bars in Specimen #1 (see Table 2.5).

3.3.5 Extent of plastic zone

The plastic zone is defined as the region in which the tensile strains in the longitudinal bars reached or exceeded the yield strain of 0.0023. Figure 3.32 shows that at a drift of 4%, the plastic zone of Specimen #1 covered a distance of 3 ft. from the base of the pile. This is about 1.3 times the pile diameter. Figure 3.33 shows that at 4% drift, the tensile strains measured at 3 ft. from the base of Specimen #2 exceeded the yield strain. In fact, the tensile strain in the bar closest to the north face (bar #4) at this height reached 0.007. By extrapolating the strain in this bar, it can be estimated that the plastic zone of Specimen #2 was about 3.5 ft., which is 1.5 times the pile diameter. As shown in Figure 3.34 and Figure 3.35, the lengths of the plastic zones of both specimens did not have significant changes at 8% drift.

Specimen #1 had its concrete cover spalling occurring over a distance of 2 ft. from the base as shown in Figure 3.12, while Specimen #2 had the concrete spalling occurring over a distance of 3 ft. as shown in

Figure 3.25. These distances are comparable to the extent of plastic deformation in the longitudinal reinforcement.

3.3.6 Plastic strain penetration

Figure 3.30 through Figure 3.35 also show the tensile strains in the longitudinal bars inside the footings of the pile specimens up to a depth of 2.25 ft. Figure 3.30 shows that at 1% drift, the tensile strains in the #11 longitudinal bars in Specimen #1 at a distance of 1.25 ft. (11 times the bar diameter, d_b) below the top face of the footing were lower than the yield strain of 0.0023. As shown in Figure 3.32b, at -4% drift, one bar (bar #5) in Specimen #1 yielded reaching a tensile strain of 0.0042 at the distance of 1.25 ft. below the top face of the footing. Figure 3.34 shows that the plastic strain penetration in the #11 bars exceeded 1.25 ft. (11 d_b) but was less than 2.25 ft. (19 d_b) at 8% drift.

Figure 3.33 shows that the tensile strains in the #9 longitudinal bars in Specimen #2 were below the yield strain at 4% drift. At -8% drift, the tensile strain in one bar (bar #5) at a depth of 1.25 ft. exceeded the yield strain, as shown in Figure 3.35b. Hence, the plastic strain penetration was deeper than 1.25 ft. (13 d_b). The generally lower plastic strain penetration observed in this specimen as compared to that in Specimen #1 is consistent with the higher tensile strains observed at the base of this pile specimen. As discussed before, this was because of the lower demand on the bond stress for the smaller diameter bars in Specimen #2.

3.3.7 Strains in confining hoops

Figure 3.36 and Figure 3.37 show the tensile strains in the hoops in Specimens #1 and #2, respectively. The positions of the strain gages are shown in Figure 2.16. As shown, the hoop strains remained small for both specimens, with some gages measuring tensile strains higher than the yield value when the drift exceeded 6%. Figure 3.36 shows that one hoop in Specimen #2 had a tensile strain of 0.006 at 8% drift. The strain level measured is consistent with the fact that no hoop fracture was observed in the tests.

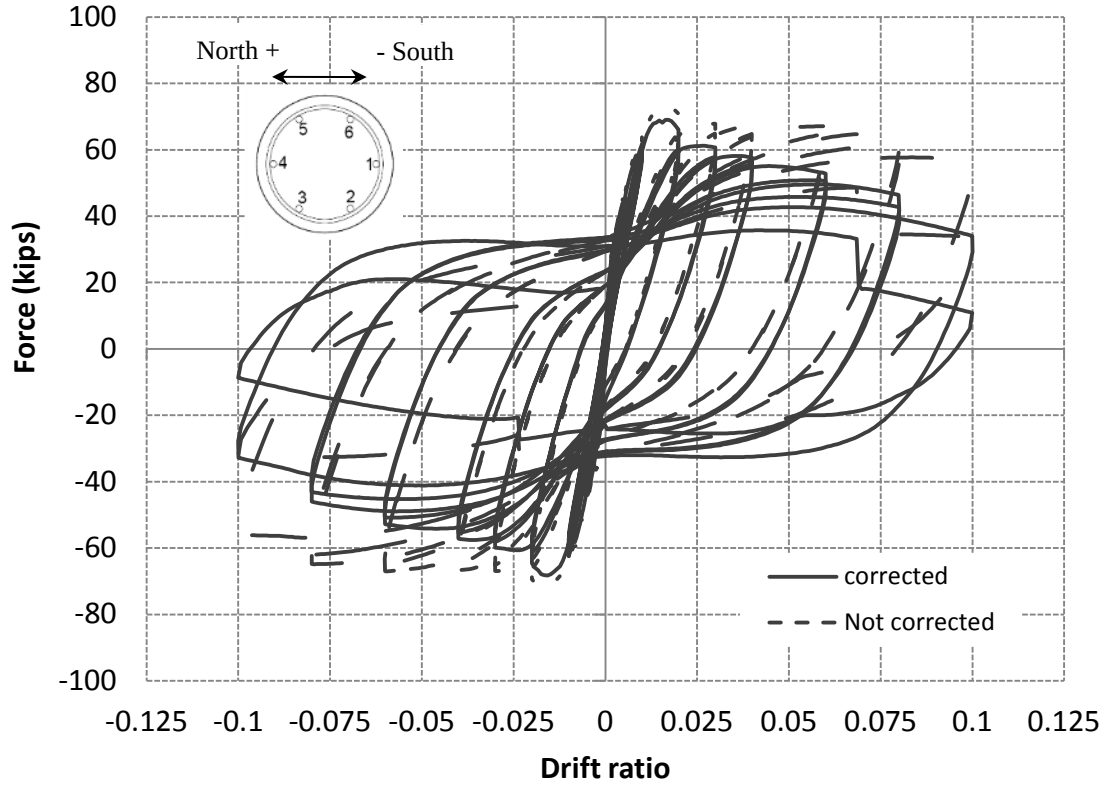

Figure 3.1 – Lateral load-vs.-drift ratio plots for Specimen #1

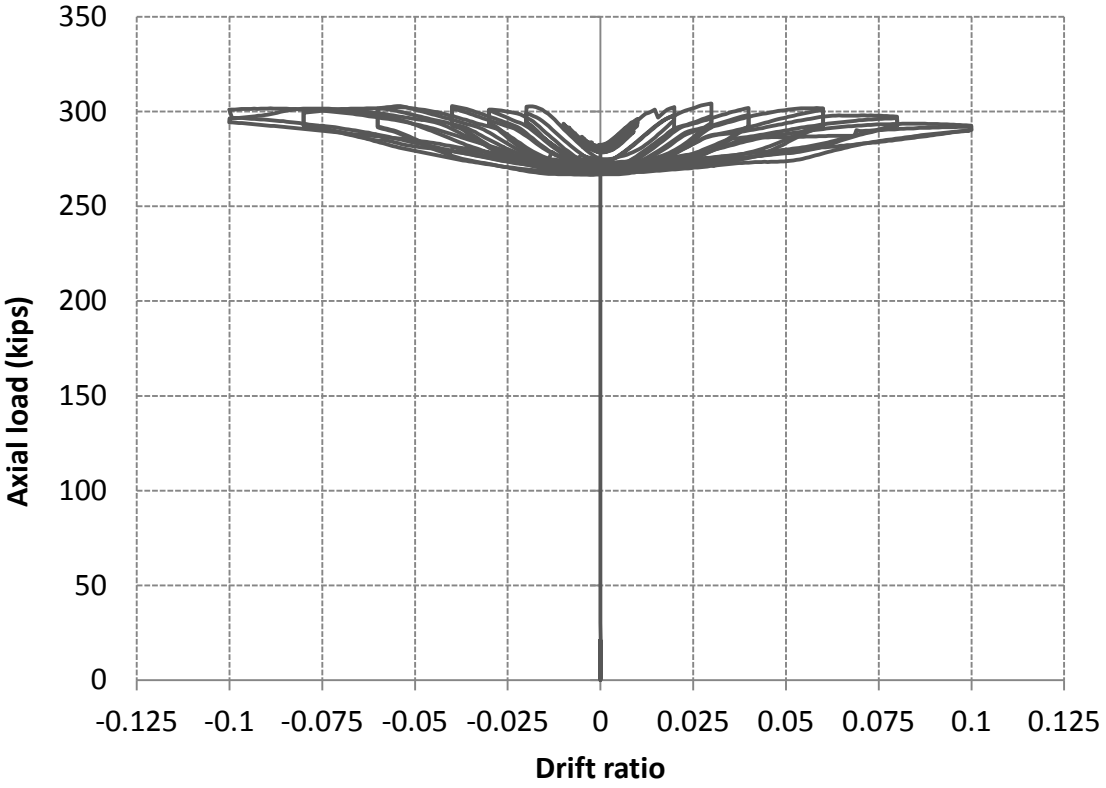

Figure 3.2 – Axial load-vs.-drift ratio plot for Specimen #1

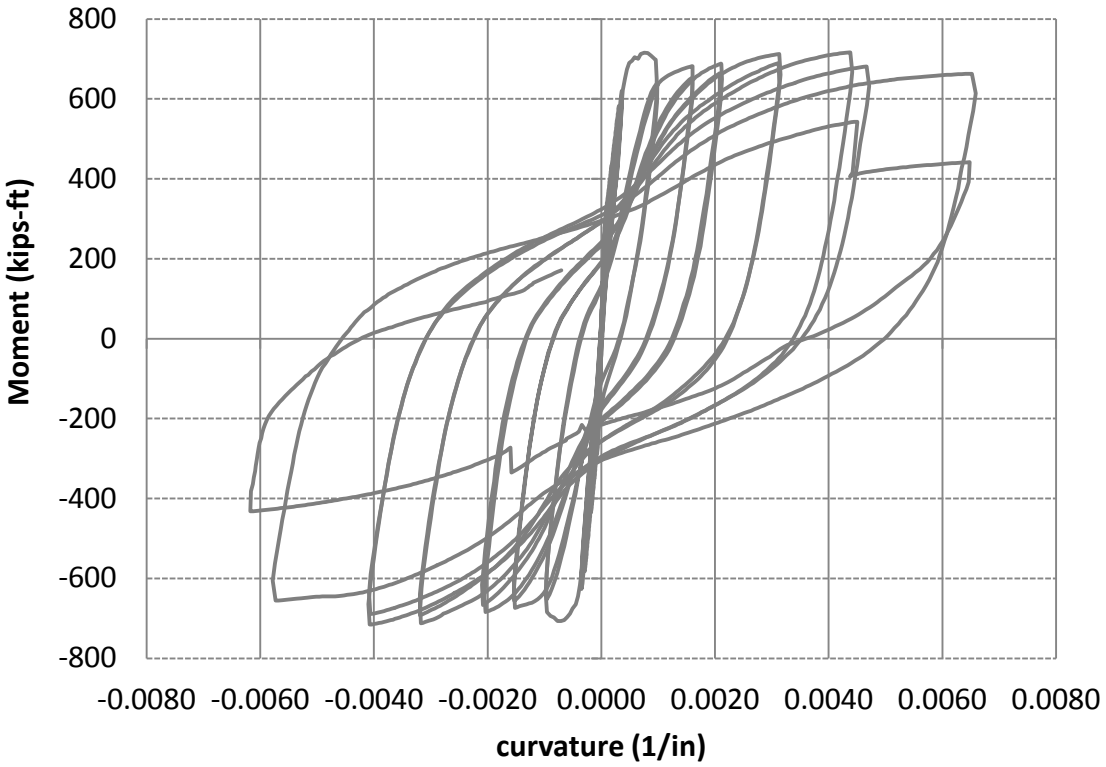

Figure 3.3 – Moment-vs.-curvature plot for Specimen #1 (average curvature over 1 ft. height from base)

(a) South face (b) North face

Figure 3.4 – Specimen #1 at 1% drift

Figure 3.5 – Specimen #1 at 2% drift

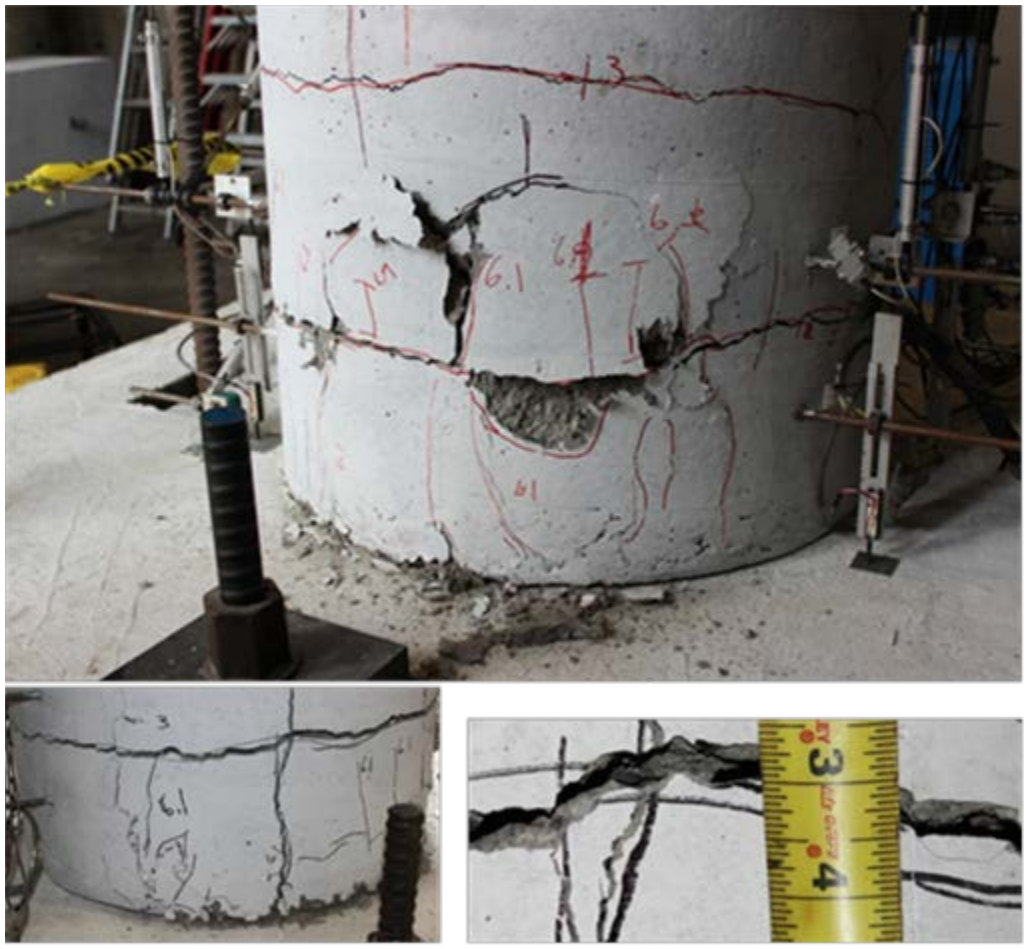

Figure 3.6 - Specimen #1 at 3% drift

Figure 3.7 – Specimen #1 at 6% drift

Figure 3.8 – Buckled bar #1 at south face of Specimen #1 during 2nd cycle of -8% drift

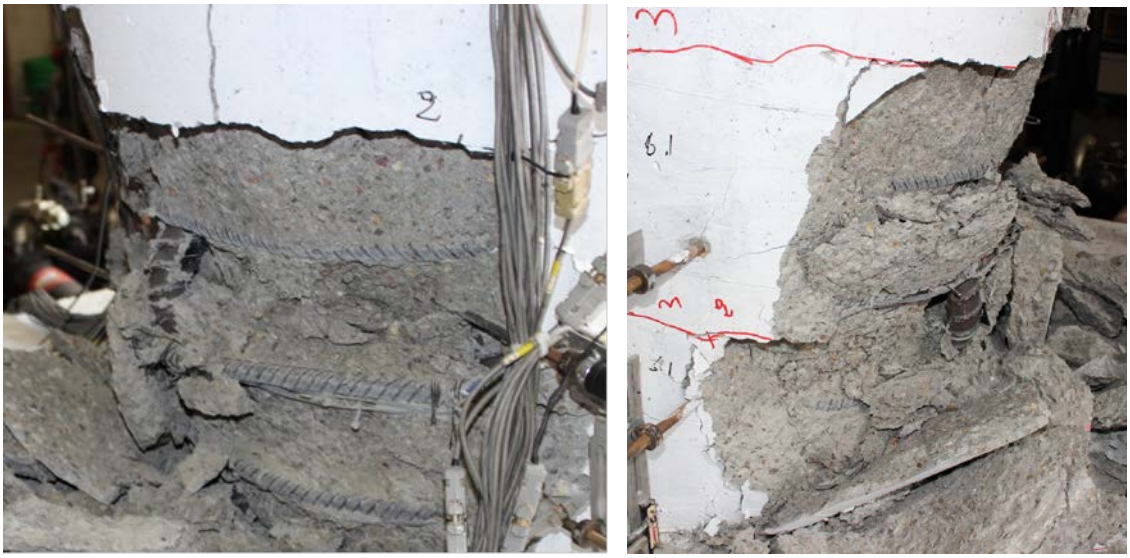

(a) South face (b) North face

Figure 3.9 – Crushing in Specimen #1 during 1st cycle of 10% drift

(a) South face (b) North face

Figure 3.10 – Crushing in Specimen #1 during 2nd cycle of +10% drift

Figure 3.11 – Fractured bar #4 at north face of Specimen #1 during 2nd cycle of -10% drift

Figure 3.12 – Specimen #1 at the end of testing

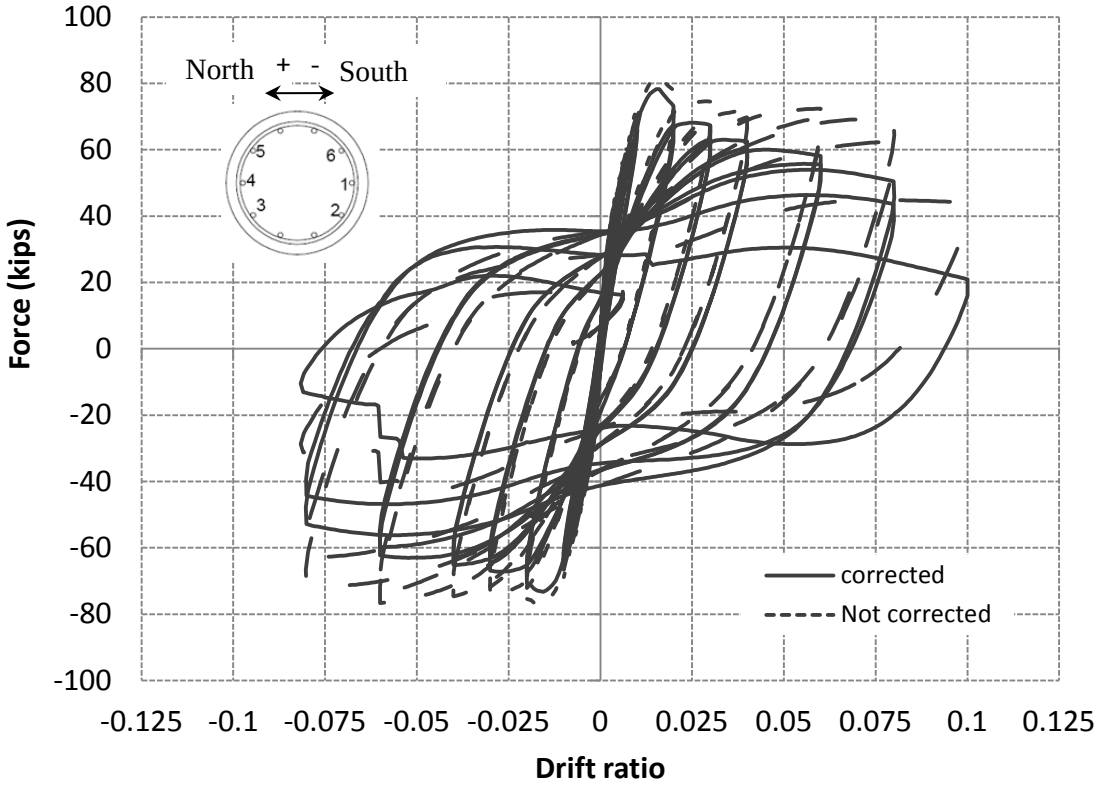

Figure 3.13 - Lateral load-vs.-drift ratio plots for Specimen #2

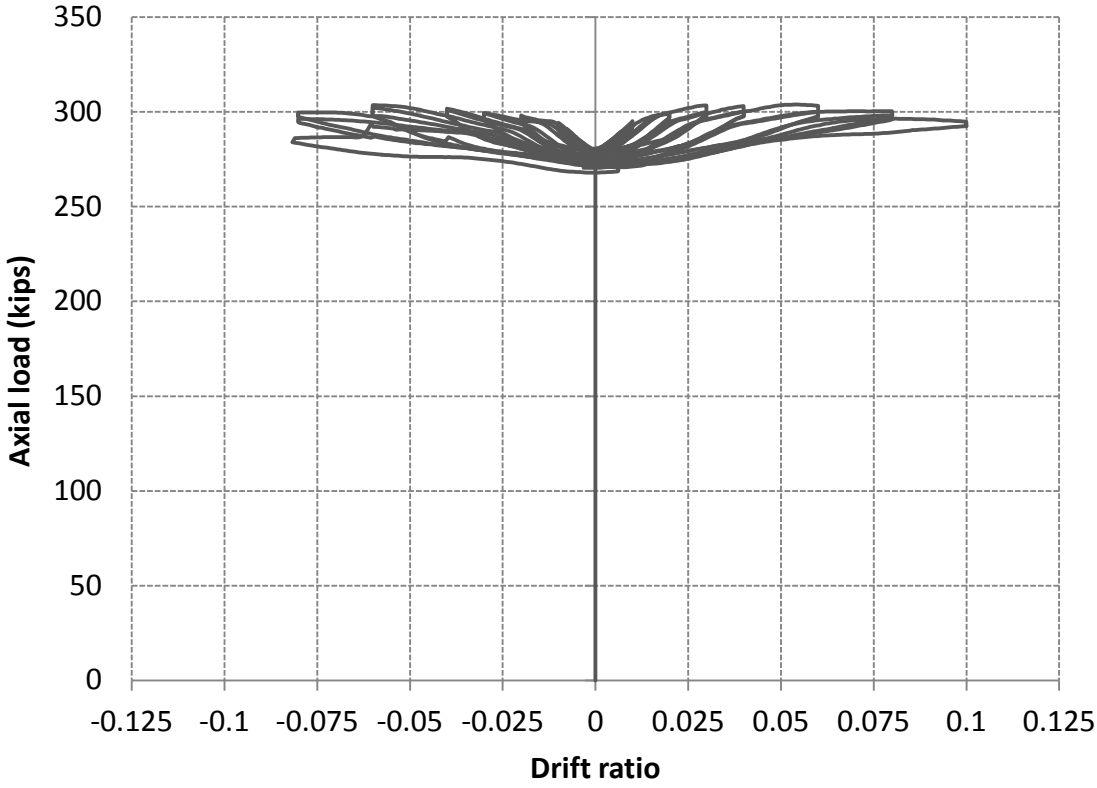

Figure 3.14 – Axial load-vs.-drift ratio plot for Specimen #2

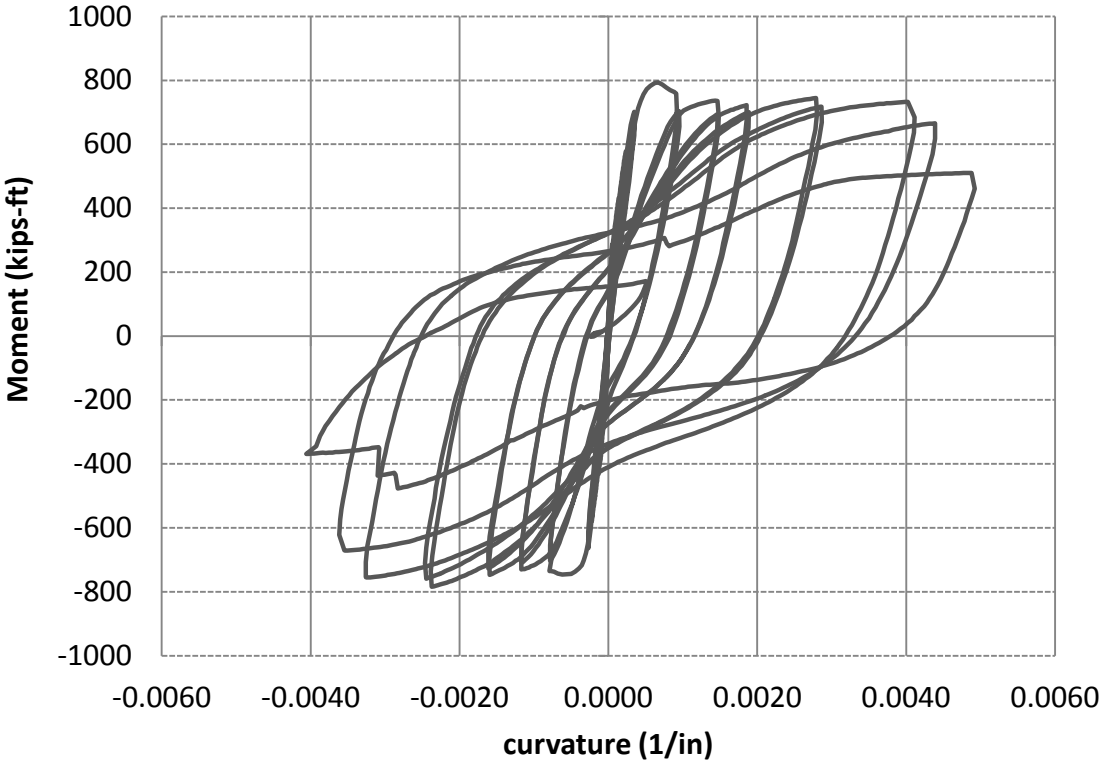

Figure 3.15 - Moment-vs.-curvature plot for Specimen #2 (average curvature over 1 ft. height from base)

(a) South face (b) North face

Figure 3.16 – Specimen #2 at 1% drift

(a) North face (b) South face

Figure 3.17 - Specimen #2 at 2% drift

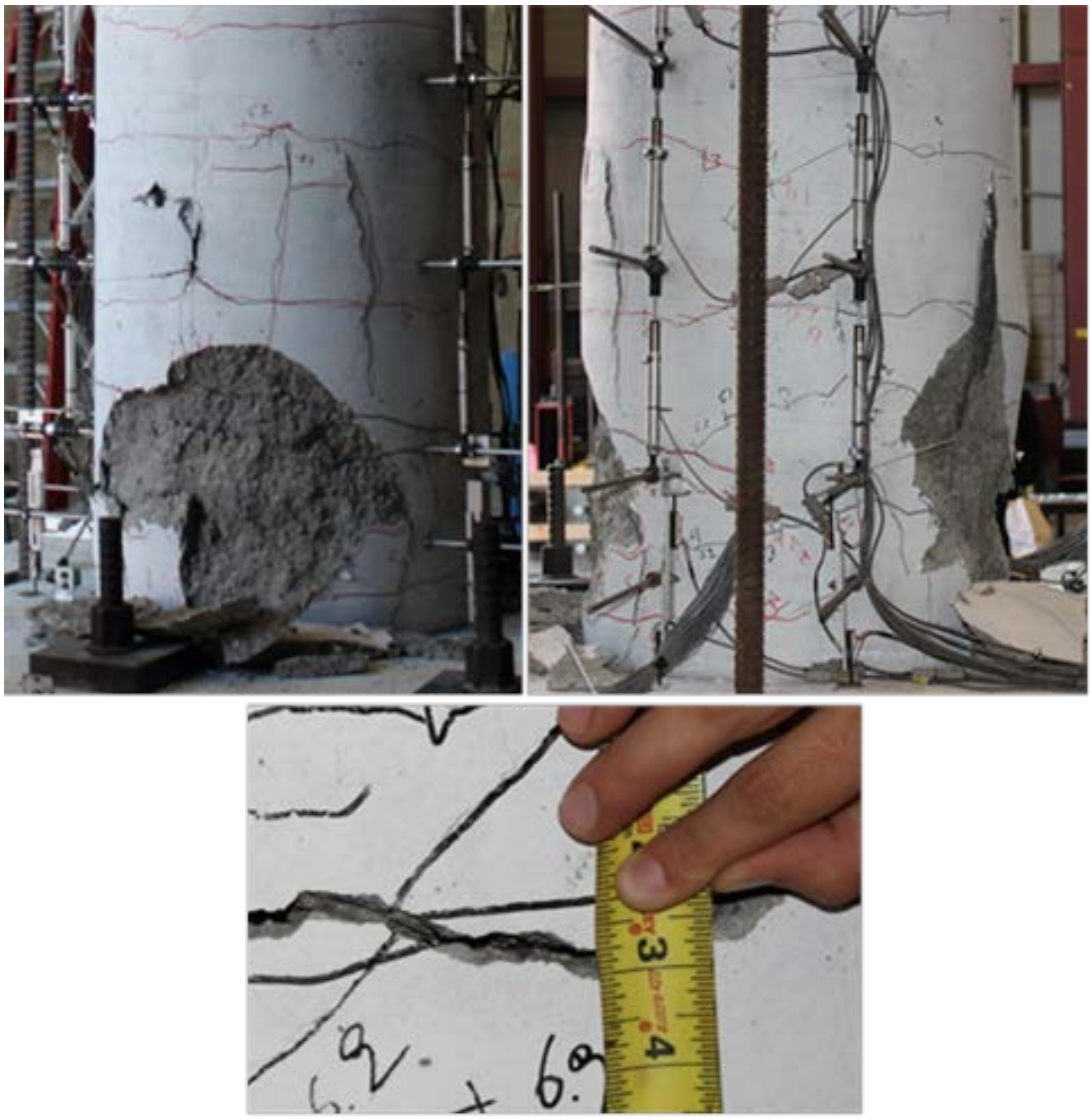

Figure 3.18 - Specimen #2 at 3% drift

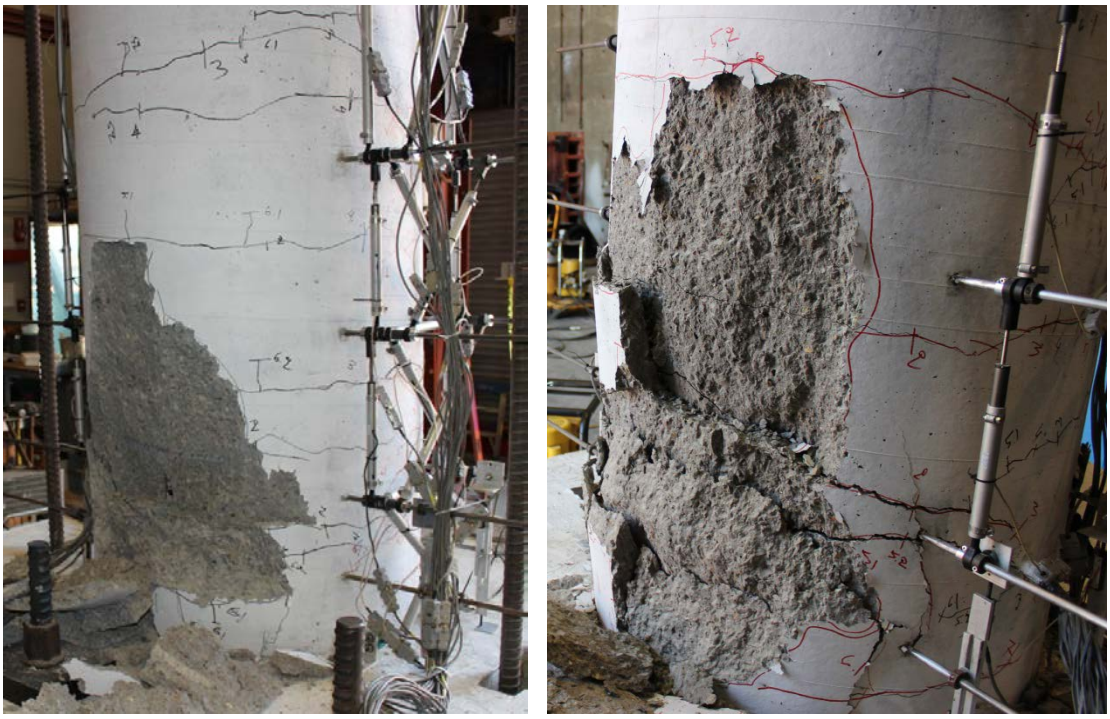

(a) South face (b) North face

Figure 3.19 –Specimen #2 at 4% drift

Figure 3.20 - Specimen #2 at 6% drift

(a) South face (b) North face

Figure 3.21 – Crushing in Specimen #2 at 1st cycle of 8% drift

(a) South face (b) North face

Figure 3.22 – Crushing in Specimen #2 at 2nd cycle of 8% drift

(a) South face (b) North face

Figure 3.23 – Fracture of bar #1 in Specimen #2 during 1st cycle of +10% drift

(a) South face (b) North face

Figure 3.24 – Fractured bars in Specimen #2 during 1st cycle of -10% drift

Figure 3.25 – Specimen #2 at the end of testing

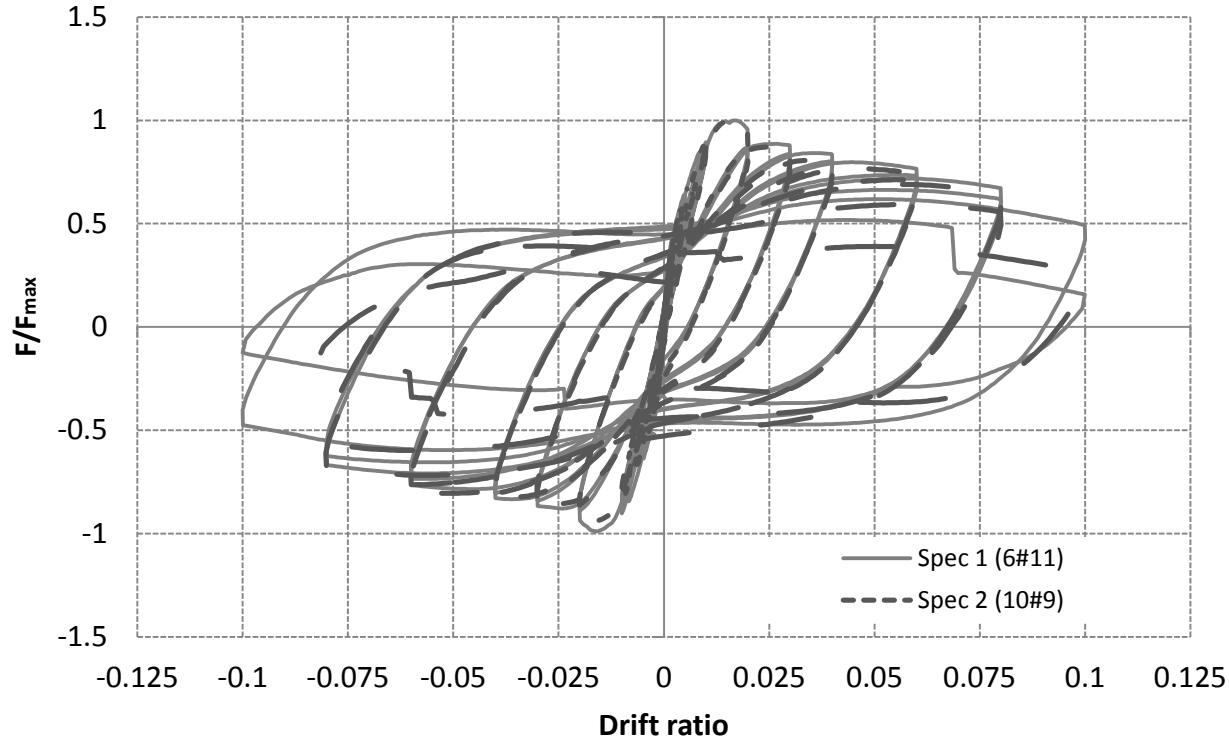

Figure 3.26 – Normalized lateral force-vs.-drift ratio curves for Specimens #1and #2

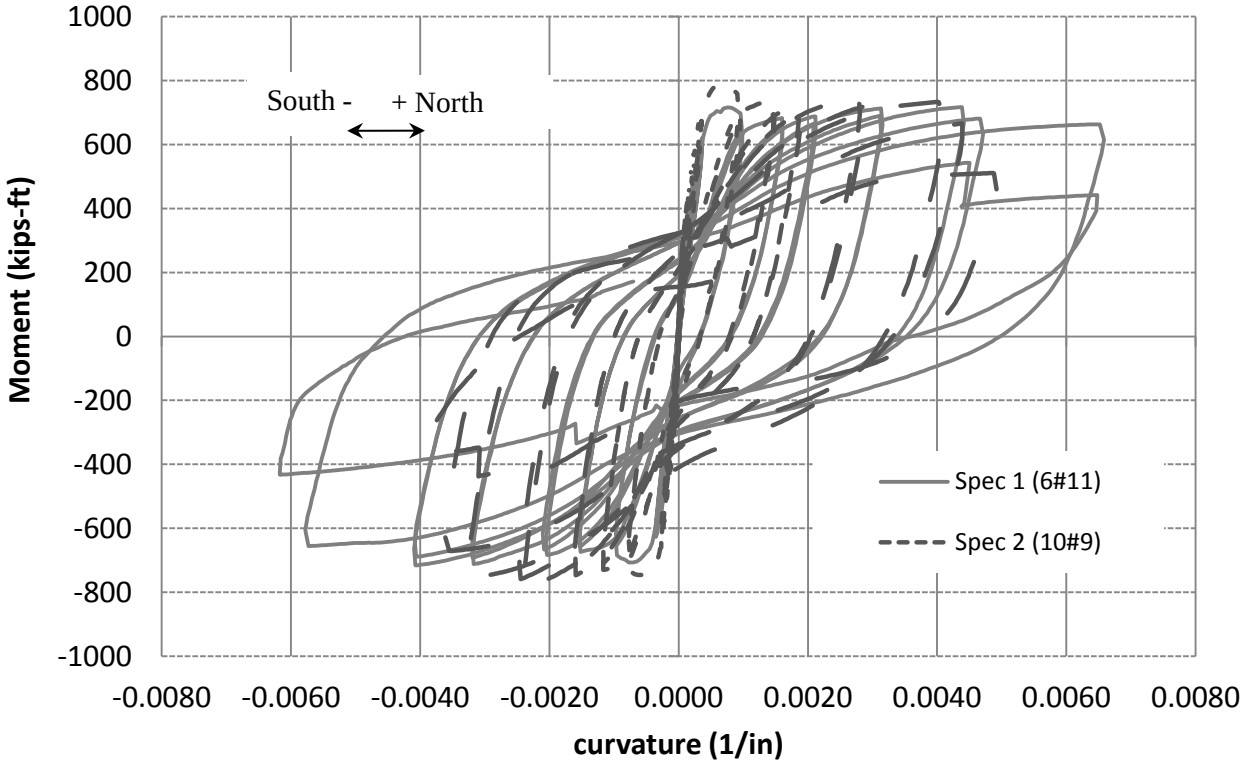

Figure 3.27 – Moment-vs.-curvature curves for Specimens #1 and #2

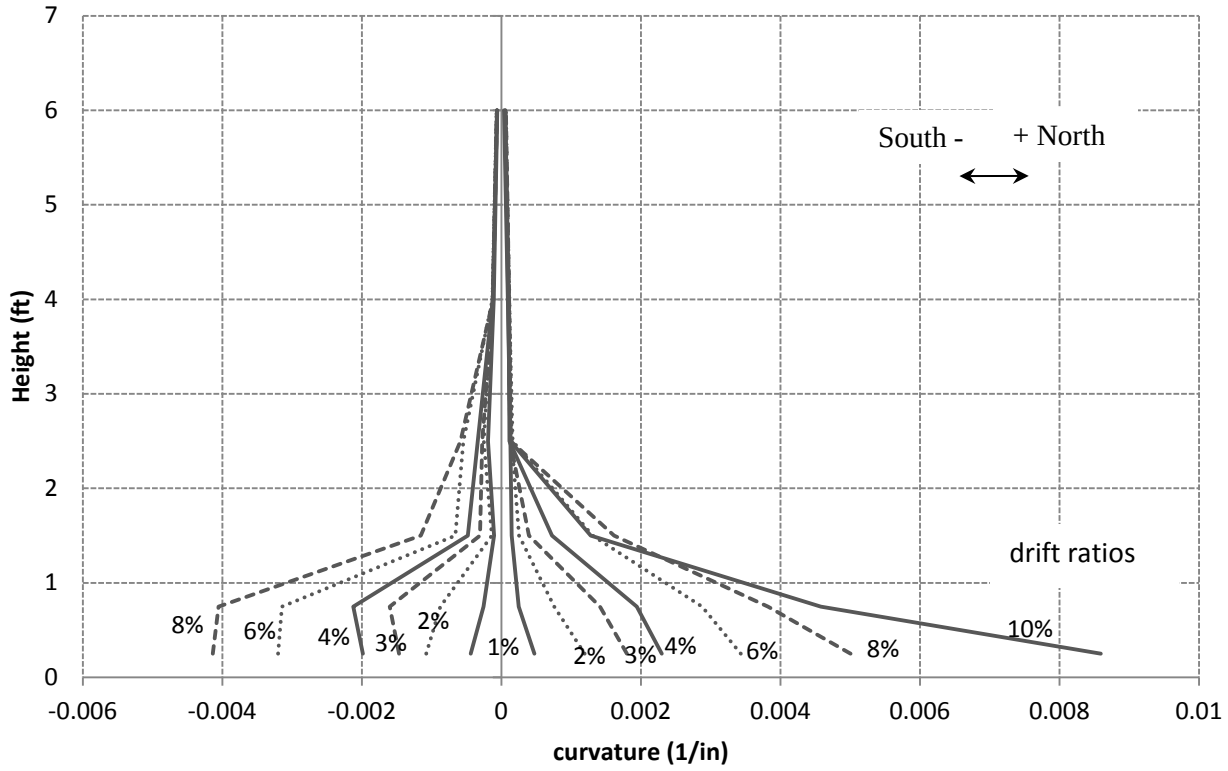

Figure 3.28 – Curvature along the height of Specimen #1

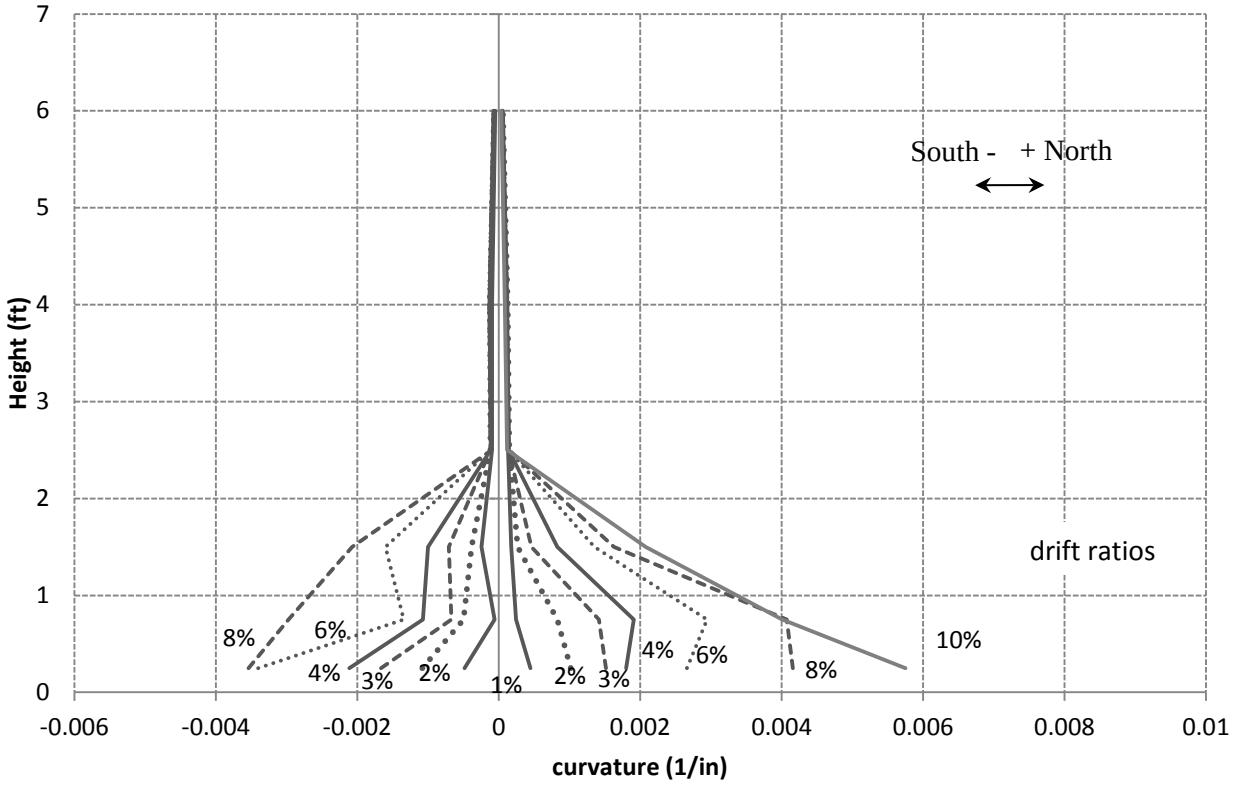

Figure 3.29 – Curvature along the height of Specimen #2

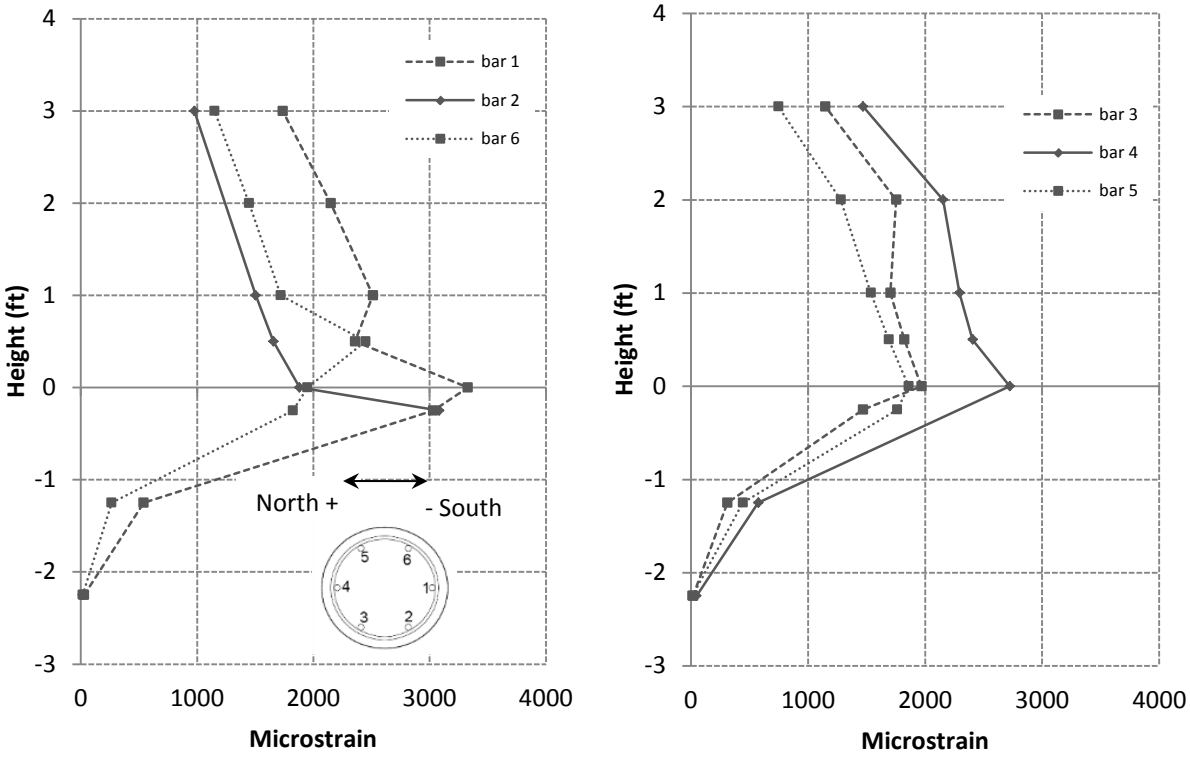

(a) +1% drift (b) -1% drift

Figure 3.30 - Tensile strains in longitudinal bars of Specimen #1 at 1% drift

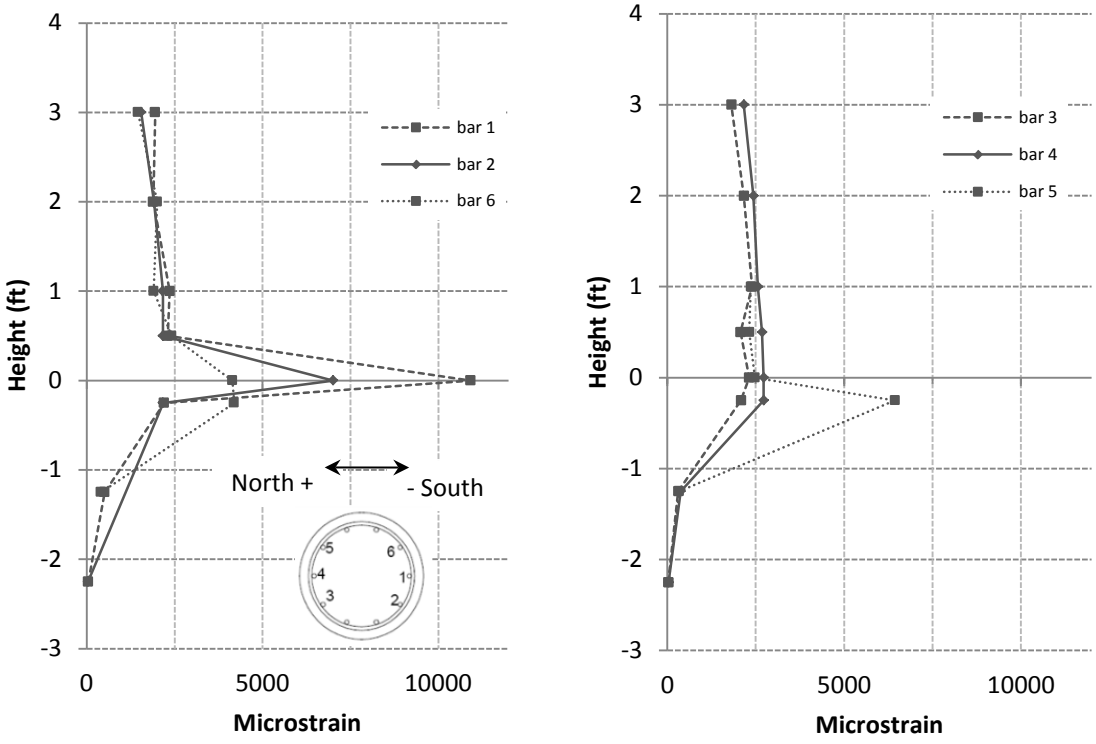

(a) +1% drift (b) -1% drift

Figure 3.31 - Tensile strains in longitudinal bars of Specimen #2 at 1% drift

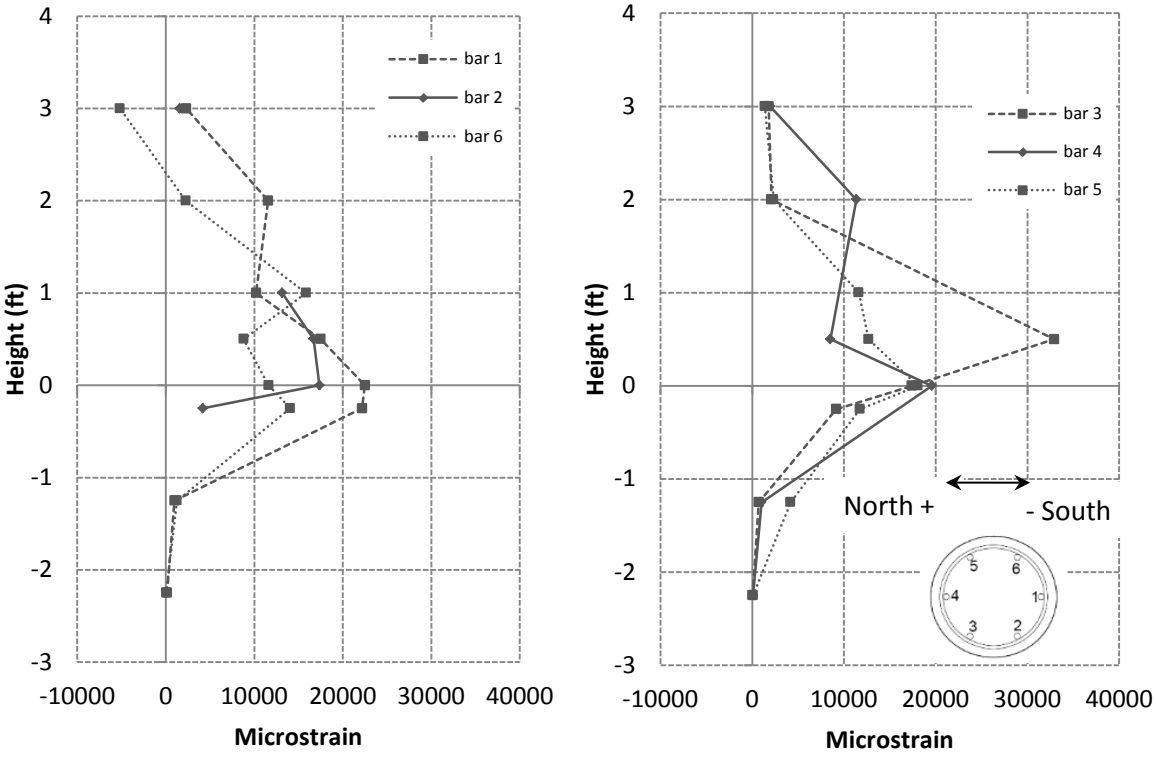

(a) +4% drift (b) -4% drift

Figure 3.32 - Tensile strains in longitudinal bars of Specimen #1 at 4% drift

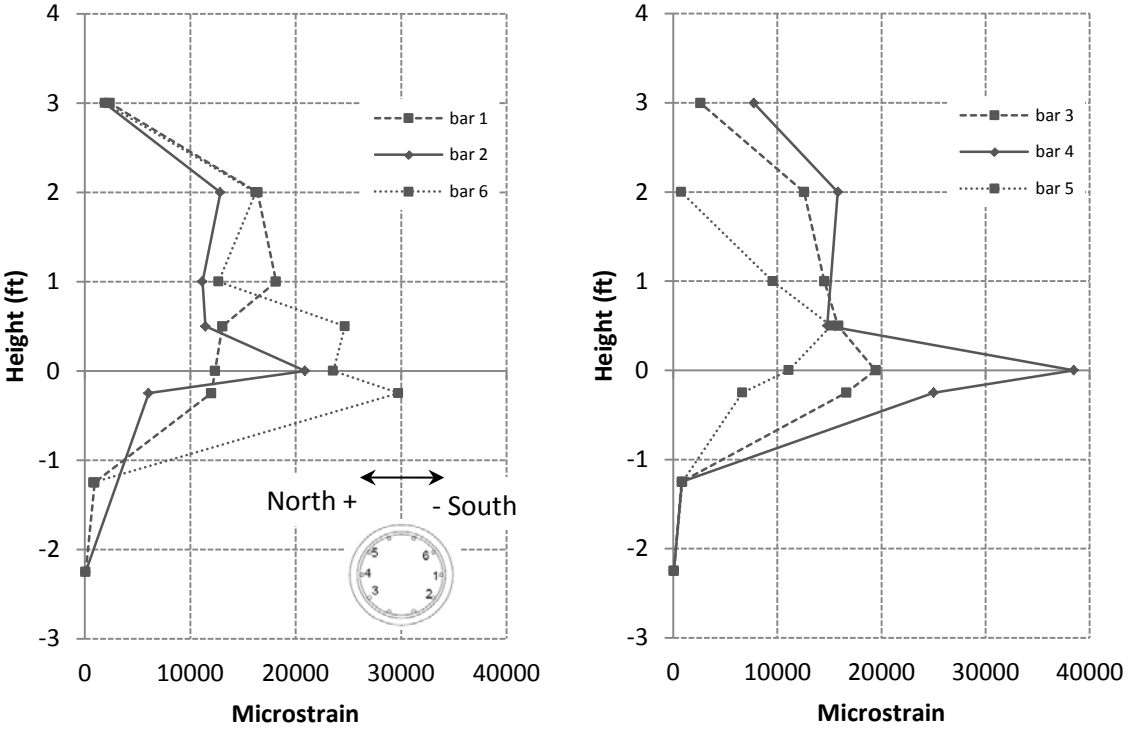

(a) +4% drift (b) -4% drift

Figure 3.33 - Tensile strains in longitudinal bars of Specimen #2 at 4% drift

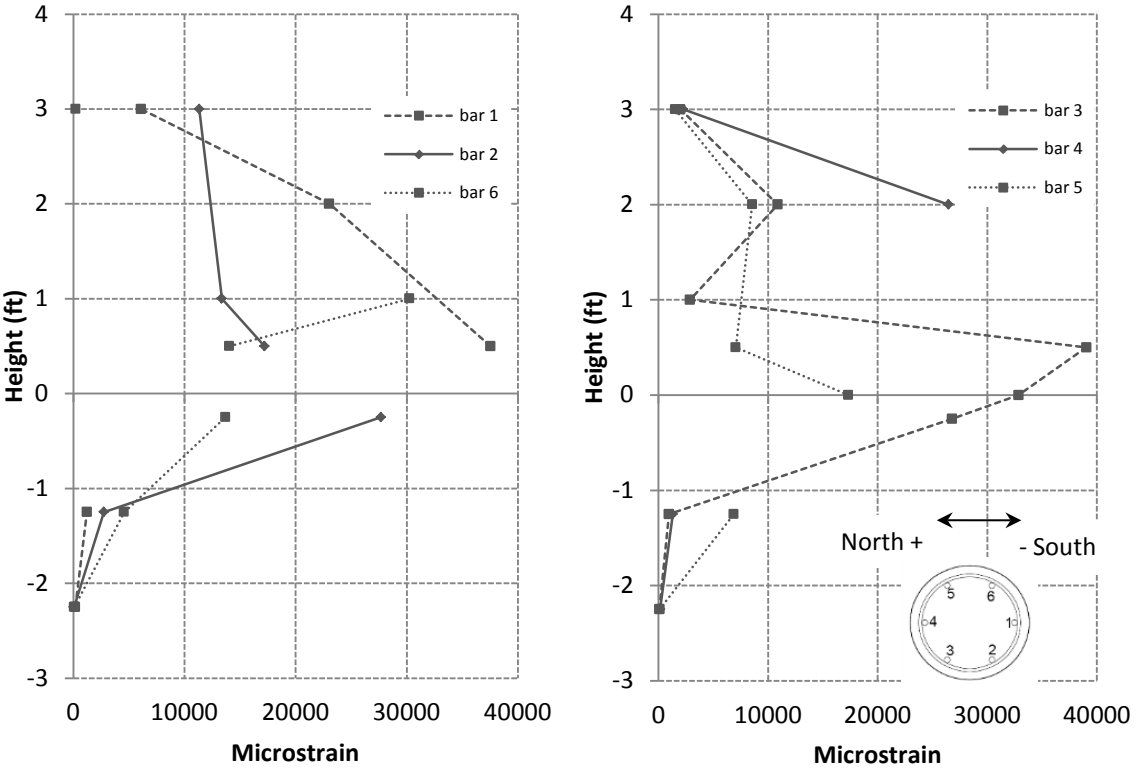

(a) +8% drift (b) -8% drift

Figure 3.34 - Tensile strains in longitudinal bars of Specimen #1 at 8% drift

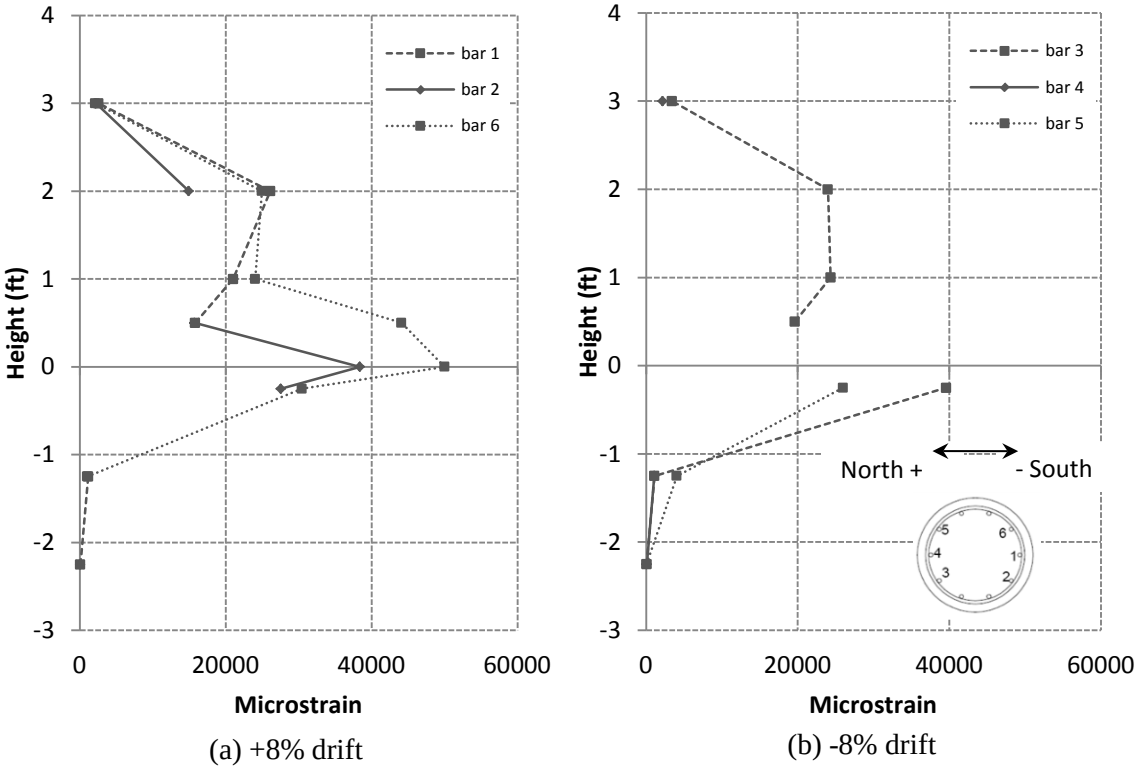

(a) +8% drift (b) -8% drift

Figure 3.35 - Tensile strains in longitudinal bars of Specimen #2 at 8% drift

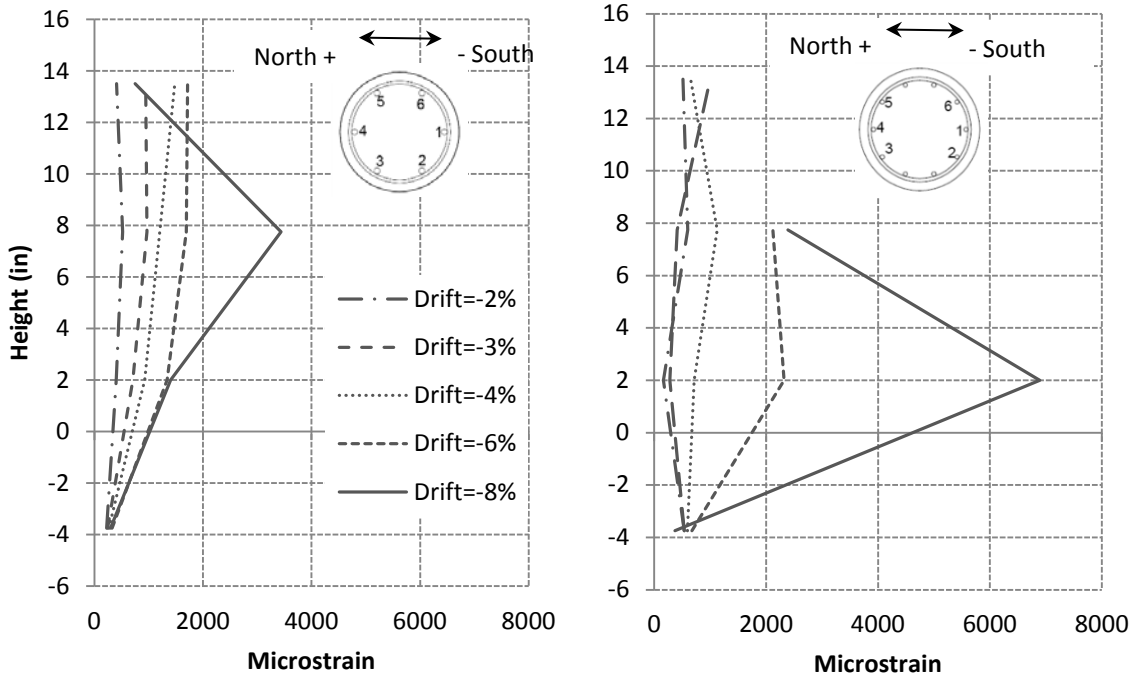

(a) Specimen #1 (b) Specimen #2

Figure 3.36 – Tensile strains in hoops near south face at different drift levels

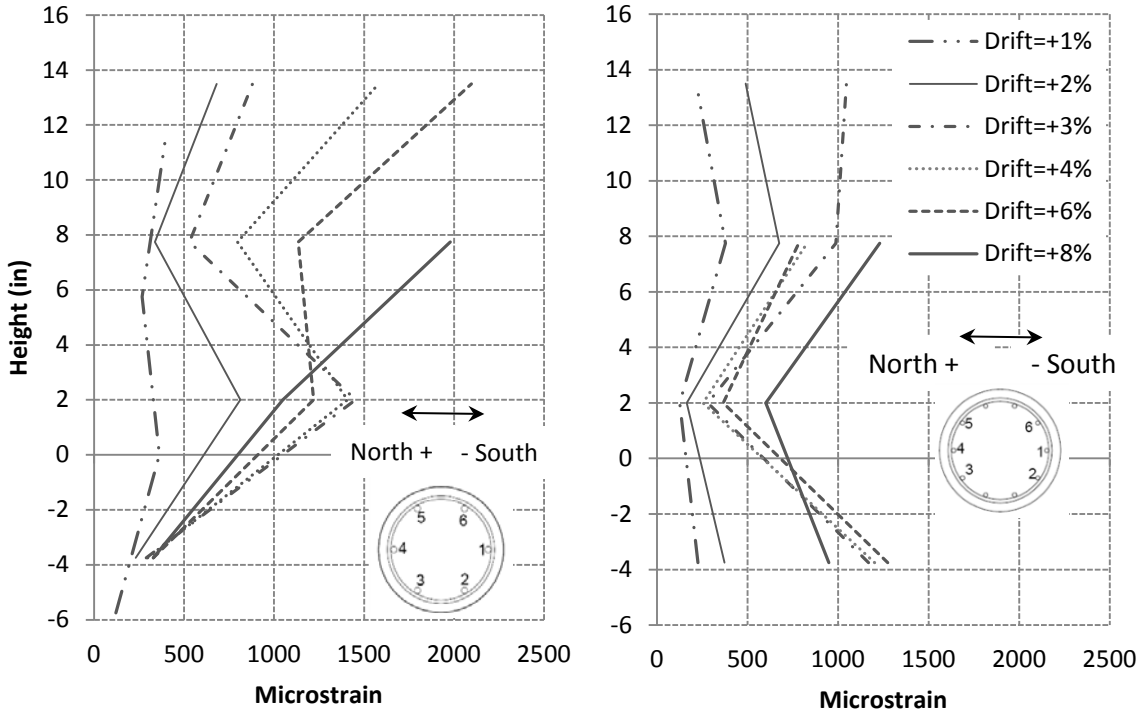

(a) Specimen #1 (b) Specimen #2

Figure 3.37 – Tensile strains in hoops near north face at different drift levels

4 Summary and Conclusions

This report presents an experimental study that investigated the effect of the circumferential spacing of longitudinal reinforcement in CIDH piles on their structural performance. In this study, two 28-in.-diameter piles were tested. Except for the spacing of the longitudinal reinforcement in Specimen #1, the design details of both specimens satisfied the Caltrans Bridge Design Specifications (Caltrans 2003) and the AASHTO LRFD Bridge Design Specifications (AASHTO 2010). The specimens had the same quantity and spacing of transverse reinforcement and similar quantities of longitudinal reinforcement. Specimen #1 had 6 #11 bars spaced at 11 in. on center, resulting in a longitudinal steel ratio of 1.52%. The bar spacing exceeded the 8-in. maximum permitted by the Caltrans and AASHTO specifications. Specimen #2 had 10 #9 bars spaced at 6.75 in. on center, resulting in a longitudinal steel ratio of 1.62%. The main observations and conclusions are summarized below.

4.1 Ductility under lateral cyclic loading

The test results have shown that the large spacing of the longitudinal reinforcement exceeding 8 in. in Specimen #1 had no detrimental effect on the ductility and the lateral load-vs.-lateral displacement behavior of the pile. The lateral load-vs.-lateral displacement curves of Specimens #1 and #2 are almost identical up to the drift level of 8%. Nevertheless, Specimen #2 exhibited a significant load degradation in the 1st cycle of 10% drift, caused by the fracture of the longitudinal bars, while that for Specimen #1 occurred in the 2nd cycle of 10% drift. Hence, Specimen #1 was slightly more ductile than Specimen #2 even though its longitudinal bars were spaced farther apart. This difference is largely attributed to the fact that the longitudinal bars of Specimen #1 had a larger diameter and were therefore more resistant to buckling after the spalling of the cover concrete. Bar buckling was responsible for the fracture of the longitudinal bars. The lateral load resistance of the two pile specimens exhibited a mild degradation after passing a drift ratio of 1% due to the P-Δ effect of the vertical load. However, both specimens showed very ductile behavior with no noticeable strength degradation in the moment-vs.-curvature relations till the fracture of longitudinal bars occurred.

Both specimens had severe crushing in the concrete core adjacent to the steel cage prior to bar buckling. Crushing was most severe at the section 10 in. above the base for both pile specimens. Specimen #1 had plastic deformation more concentrated near the base as compared to Specimen #2. This led to a higher curvature measured near the base of Specimen #1 at comparable drift levels. Specimen #1 also had a slightly shorter plastic zone, which is defined as the region in which the tensile strains in the longitudinal bars reached or exceeded the yield strain, and had smaller plastic strains in the longitudinal bars. The cover concrete in Specimen #1 spalled over a distance of 2 ft. from the base, while that in Specimen #2 spalled over a distance of 3 ft.

4.2 Flexural crack pattern

Specimen #1 had flexural cracks spaced farther apart and larger crack widths than Specimen #2. The distances of flexural cracks in Specimen #1 were 6 to 9 in., while those in Specimen #2 were 9 to 12 in. At 1% drift, at which the longitudinal bars in the piles started to yield, the flexural cracks in Specimen #1 had propagated around half of the circumference of the pile, while those in Specimen #2 did not propagate as far. However, for both specimens, the crack widths remained small at this drift level.

4.3 Conclusions

The spacing of longitudinal bars in circular RC members can be larger than 8 in. without jeopardizing the structural performance of the member. This spacing does not seem to affect the effectiveness of the confinement on the concrete core. However, the diameter of longitudinal bars can affect the ductility of a laterally loaded member. Larger-diameter bars are more resistant to bucking for the same spacing of the transverse reinforcement, and can therefore lead to more ductile flexural behavior. The limited experimental data also show that the spacing and the size of longitudinal bars may affect the extent of the plastic zone of a laterally loaded member, in which flexural cracking, concrete spalling, and the yielding of the longitudinal bars occur. The specimen with larger-diameter longitudinal bars and larger bar spacing had more concentrated plastic deformation near the base. The underlying reason for this needs to be further studied. However, one possible explanation is that smaller-diameter bars have a lower bond stress

demand and therefore less bond slip. This leads to higher strains and therefore higher stresses in the bars in the vicinity of flexural cracks. The higher bar stresses can lead to a more uniform distribution of pile curvature. Finally, the spacing and the size of longitudinal bars have a clear influence on the spacing and the width of flexural cracks, which is a well-known fact.

References

Alter, J.K. (2011), "Technical Note: Hollow Threaded Rebar for Cross Hole Sonic Logging Access Tubes Combined with Longitudinal Concrete Reinforcing in Drilled Shafts", *DFI Journal*, Vol. 5, No. 2.

AASHTO (2010), *AASHTO LRFD Bridge Design Specifications*, 5th Edition, American Association of State Highway and Transportation Officials, Washington, DC.

ASTM (2009), *ASTM A706/A706M-09b Standard Specification for Low-Alloy Steel Deformed and Plain Bars for Concrete Reinforcement*, ASTM International, West Conshohocken, PA.

Caltrans (2003), *Bridge Design Specifications*, California Department of Transportation, Sacramento, CA.

Mander, J. B., Priestley, M. J. N., Park, R. (1988a), "Theoretical Stress-Strain Model for Confined Concrete" *Journal of Structural Engineering*, Vol. 114, No. 8, pp. 1804-1826.

Mander, J. B., Priestley, M. J. N., Park, R. (1988b), "Observed Stress-Strain Behavior of Confined Concrete" *Journal of Structural Engineering*, Vol. 114, No. 8, pp. 1827-1849.

Paulay, T., Priestley, M. J. N. (1992), *Seismic Design of Reinforced Concrete and Masonry Buildings*, John Wiley & Sons, Inc.